Department of Naval Architecture

and Marine Engineering

AN IMPROVED AXIAL-FLOW SIREN FOR FATIGUE TESTING GAS TURBINE BLADES

by

THOMAS FRANCIS DONNELLY, JR.

and

JAMES ALBERT PALMER, JR.

May, 1965

AN IMPROVED AXIAL-FLOW SIREN FOR FATIGUE TESTING GAS TURBINE BLADES

by

THOMAS FRANCIS DONNELLY, JR., Lieutenant, United States Navy
B.S., United States Naval Academy
(1957)

JAMES ALBERT PALMER, JR., Lieutenant, United States Navy
B.S., United States Naval Academy
(1958)

SUBMITTED IN PARTIAL FULFILLMENT

OF THE REQUIREMENTS FOR THE DEGREE OF

NAVAL ENGINEER

AND THE DEGREE OF

MASTER OF SCIENCE IN NAVAL ARCHITECTURE

at the

MASSACHUSETTS INSTITUTE OF TECHNOLOGY

May, 1965

Signature of Authors . . . . . .

. . . . . .
Department of Naval Architecture
and Marine Engineering, 21 May 1965

Certified by . . . . . .
Thesis Supervisor

Accepted by . . . . . .
Chairman, Departmental Committee
on Graduate Students

AN IMPROVED AXIAL-FLOW SIREN FOR FATIGUE TESTING GAS TURBINE BLADES

Thomas F. Donnelly, Jr., Lieutenant, United States Navy

James A. Palmer, Jr., Lieutenant, United States Navy

Submitted to the Department of Naval Architecture and Marine Engineering on 21 May 1965 in partial fulfillment of the requirements for the Master of Science Degree in Naval Architecture and Marine Engineering and the Professional Degree, Naval Engineer

ABSTRACT

Gas turbine blades may be fatigue tested by the pulsed air technique. This method is most successful when the blade is placed in a concentrated high intensity acoustic field pulsating at a natural frequency of the blade.

The General Electric "Pulsed Air Vibration Tester," which is basically an axial-flow siren, was studied in this thesis in order to develop improvements that would extend its useful fatigue testing range to 20,000 cps. Experiments conducted on this siren revealed that at particular discrete frequencies in the range from 3,000 to 15,000 cps the intensity level was appreciably higher than at adjacent frequencies. These higher intensities were attributed to resonance which occurred in the air chamber immediately upstream of the rotating disc of the siren.

A new siren design was proposed that featured a controllable length air chamber. Thus, the chamber could be tuned to resonate at a frequency corresponding to a natural frequency of the blade, to take advantage of the higher intensity level.

This proposal was simulated by changing the dimensions of the original chamber. Test results of the new configuration confirmed expectations that resonance would occur at different frequencies. Further experiments revealed that length is the dominant dimension affecting the resonant frequency.

The only microphone available with the required frequency response was limited to sound pressure levels of 180 db. The microphone was positioned several wavelengths from the source, as dictated by this limitation. Thus, the observed results show the effect of finite amplitude attenuation and a discussion of this phenomenon as it applies to this thesis is included.

To realize the full benefit of the increased intensity level, the blade must be placed as close to the source as possible to minimize the intensity level loss from finite amplitude attenuation and spherical divergence.

Thesis Supervisor: Patrick Leehey

Title: Associate Professor of Naval Architecture

ACKNOWLEDGEMENTS

The authors wish to express their appreciation to Professor Patrick Leehey, Department of Naval Architecture and Marine Engineering, Massachusetts Institute of Technology, for his advice and guidance in the development of this thesis; to the General Electric Company, Small Aircraft Engine Department, West Lynn, Massachusetts, for providing the test apparatus; and to Mr. Joseph Bendersky and Mr. Courtenay Crocker of the General Electric Company for their assistance.

TABLE OF CONTENTS

LIST OF FIGURES

INTRODUCTION

It is of paramount importance in the production of gas turbine engines to know both the endurance limit (fatigue limit) and the operating stresses of the blades because failure could be catastrophic. For example, a blade could be subjected to a steady vibratory stress in the vicinity of one of its higher resonances. At this frequency the stress induced in the blade may be well above the endurance limit. Extended operation at this frequency will result in blade failure that, in turn, may cause engine failure.

Blade design is predicated in part on vibration analysis, but this, alone, is inadequate because the mathematical model may be somewhat unrealistic. Therefore, blade vibration testing to determine natural frequencies (corrected for the centrifugal field present in the engine) and fatigue testing to determine blade strength levels are an integral part of the manufacturing process.

Several methods are available to excite blade vibrations in the laboratory. Among them are electromagnetic excitation, mechanical flexing where the force is applied to the blade, mechanical excitation where the force is applied to the mount, jet nozzle excitation, and tuned air chambers. Each one of these methods has a particular application to which it is most ideally suited, but it cannot produce the desired vibration in all situations (11)* One method that seems to have universal application is the pulsed-air technique. It is this blade vibration testing scheme that will be investigated in this thesis.

---

* Numbers in parentheses refer to the bibliography

In this method high pressure air is exhausted through a slotted, rotating disc which is close to the stationary disc having identical slots. The alternate opening and closing of the slots produces pulsations in the air stream that impinge on a blade mounted downstream. The pulse frequency is proportional to the speed of rotation and the number of holes in the disc. The pulse intensity is a function of many factors, the most obvious of which is the spacing between the rotating and fixed discs. It will be assumed that this clearance has been reduced to the minimum possible without contact between the two adjacent surfaces and there will be no further discussion of this point. The objective of this thesis is to determine and analyze the effect of other factors on pulse intensity and, using these results, to actually improve the performance of the particular air pulse generator under study.

The Small Aircraft Engine Department of the General Electric Company made available their "pulsed-air vibration tester" for this investigation. This apparatus is basically an axial-flow siren, the frequency of which may be closely controlled from zero to fifteen thousand cycles per second. The first step in analyzing this siren was to determine how well it compared to the state of the art of siren design.

It is generally accepted that there are five fundamental criteria for a maximum efficiency siren where efficiency may be considered the ratio of acoustic power output to the air power input (5), (6), (1), (4).

1. The air flow from the siren should be exhausted through an exponential horn, the cut-off frequency of which is lower than the operating frequency of the siren, to provide a correct impedance transformation from the siren exit to the atmosphere.

2. The time for opening and closing the ports should be small compared with the time they are fully opened or fully closed because throttling is wasteful.

3. The resistance of the ports, while non-linear, is approximately proportional to flow velocity. Therefore, the change in pressure across the ports should be small.

4. To prevent reflection back through the ports, 2π times the maximum dimension of the port should be much less than the wavelength of the sound produced by the siren.

5. There should be high mass flow to obtain maximum acoustic power output.

The General Electric siren failed the first three criteria outright and met the fourth only at low frequency. However, this siren was quite effective in fatigue testing gas turbine blades at frequencies up to 7,500 cps. It was, therefore, decided that these criteria did not apply categorically to all siren design, because high efficiency may not be compatible with the fundamental purpose of the siren.

A compromise among the various criteria must be made, based on the purpose of the siren. If the siren were to be used as an alarm or warning device, maximum power output at high efficiency would be

the goal. It would be designed to operate at the optimum audible frequency, say 256 cps. Because the wavelength, λ, is large, the maximum dimension of the ports could be large and still be less than $\lambda/2\pi$. Therefore, high mass flow with small pressure drop across the ports would be possible. An efficient horn could be incorporated in the design, because the siren would operate only at this one, low frequency. As there would be no restrictions on its size and because of the low frequency operation, it would be possible to design the ports to produce a short transition time for opening and closing compared with the time they are fully opened or fully closed. This would be a highly efficient siren because all the criteria for high efficiency are compatible with the goal.

On the other hand, consider this siren. Its purpose is to fatigue test gas turbine blades. An average size gas turbine blade is approximately one and one-half inches long by five-eighths inches wide. Only that part of the acoustic pressure field that physically contacts the blade will excite it, and, for practical purposes, all the remaining area of the pressure field is wasted. The relative excitation of the blade depends on how much energy is transferred to it from the acoustic pressure field, and the pulse frequency. There is more energy available for transfer in an intense pressure field, and the intensity is proportional to the mass flow through the siren. When operated at a resonant blade frequency, a given amount of transferred energy will induce much more stress than operation at some arbitrary frequency. It takes more energy to excite the higher modes of vibration associated with high frequency resonances than to excite the fundamental

mode, because much greater damping takes place at these higher modes. Therefore, the goal of this siren design is to produce maximum acoustic intensity in a concentrated field. High mass flow is, necessarily, the pre-eminent criterion to which all other criteria must be subordinated.

Within the framework of these considerations, it is evident why the General Electric siren was not designed in accordance with the high efficiency criteria. No horn was included, possibly because of the wide frequency range over which the siren was required to operate. To confine the acoustic pressure field to a small area, it was necessary to use a siren whose physical dimensions were small. In this case, the discs are about two inches in diameter and have equally spaced radial slots about one-fourth inch long (see Figures 1, 2, 3(a) and 3(b)). The discs are identical because this configuration permits maximum mass flow and maximum frequency for a given shaft speed. Thus, the ports are always either opening or closing, and the resultant throttling loss must be accepted. To obtain maximum mass flow, the upstream pressure is always high enough to choke the flow at the ports. As a consequence, there are losses from shocks and high port resistance. At frequencies above 8,400 cps. back reflection will occur.

It may be concluded from this preliminary investigation that the General Electric siren relies solely on maximum mass flow, to the exclusion of any high efficiency features, to produce maximum intensity. It might be thought of as a "brute force" siren. The

validity of this approach will be tested experimentally, and an analysis will be made of all factors that affect intensity. Based on this analysis, design changes that do not alter the basic configuration of the siren will be made to increase its intensity and frequency range and, thereby, increase its blade fracture potential.

The pulsed-air vibration tester is known to the personnel at General Electric Company as the "air chopper." It has been analyzed in this thesis as a siren, which it is. Throughout the remainder of this thesis the terms "siren" and "air chopper" refer to the same device and will be used interchangeably.

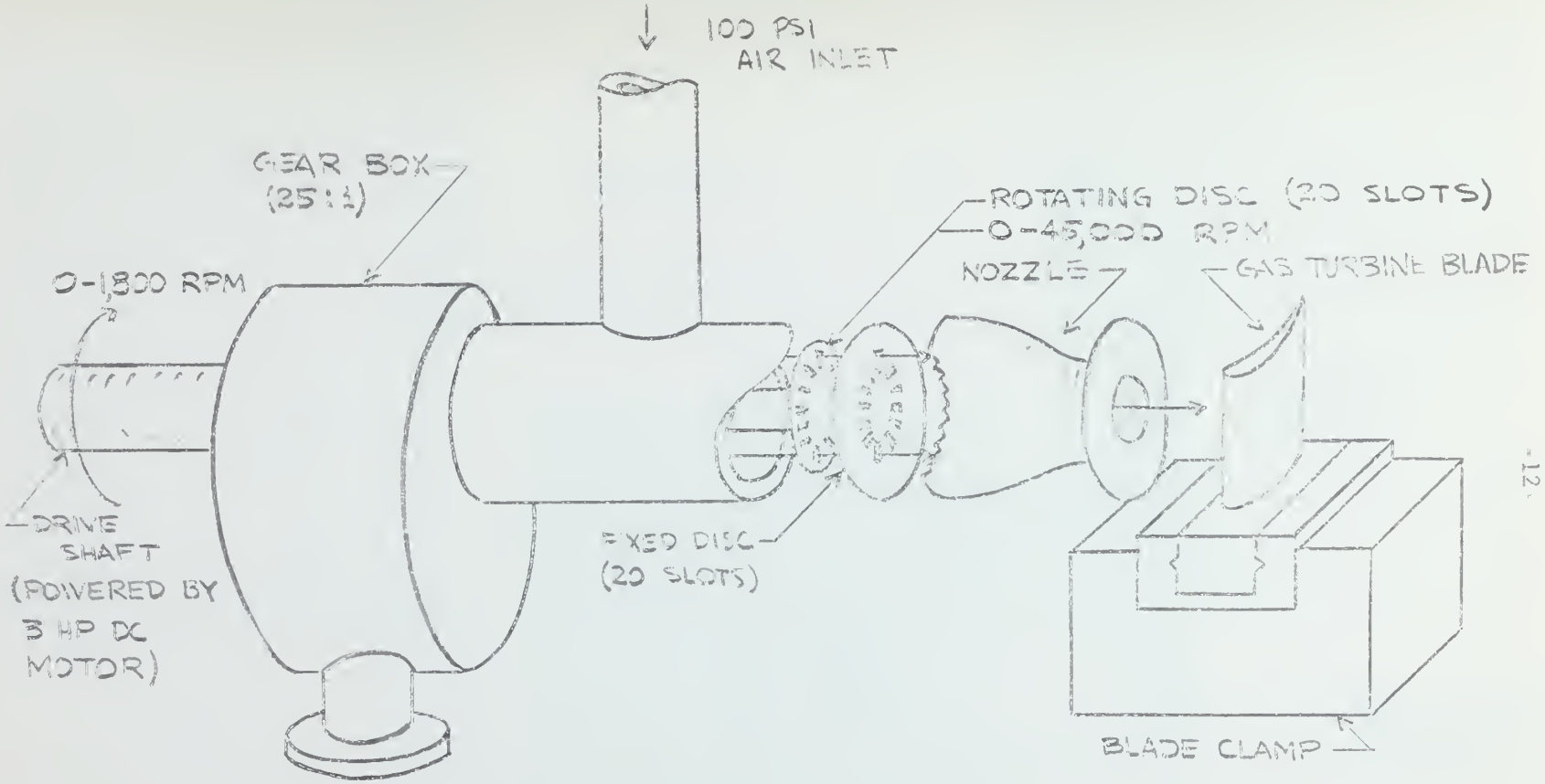

Figure 1. Schematic of Original Air-Chopper

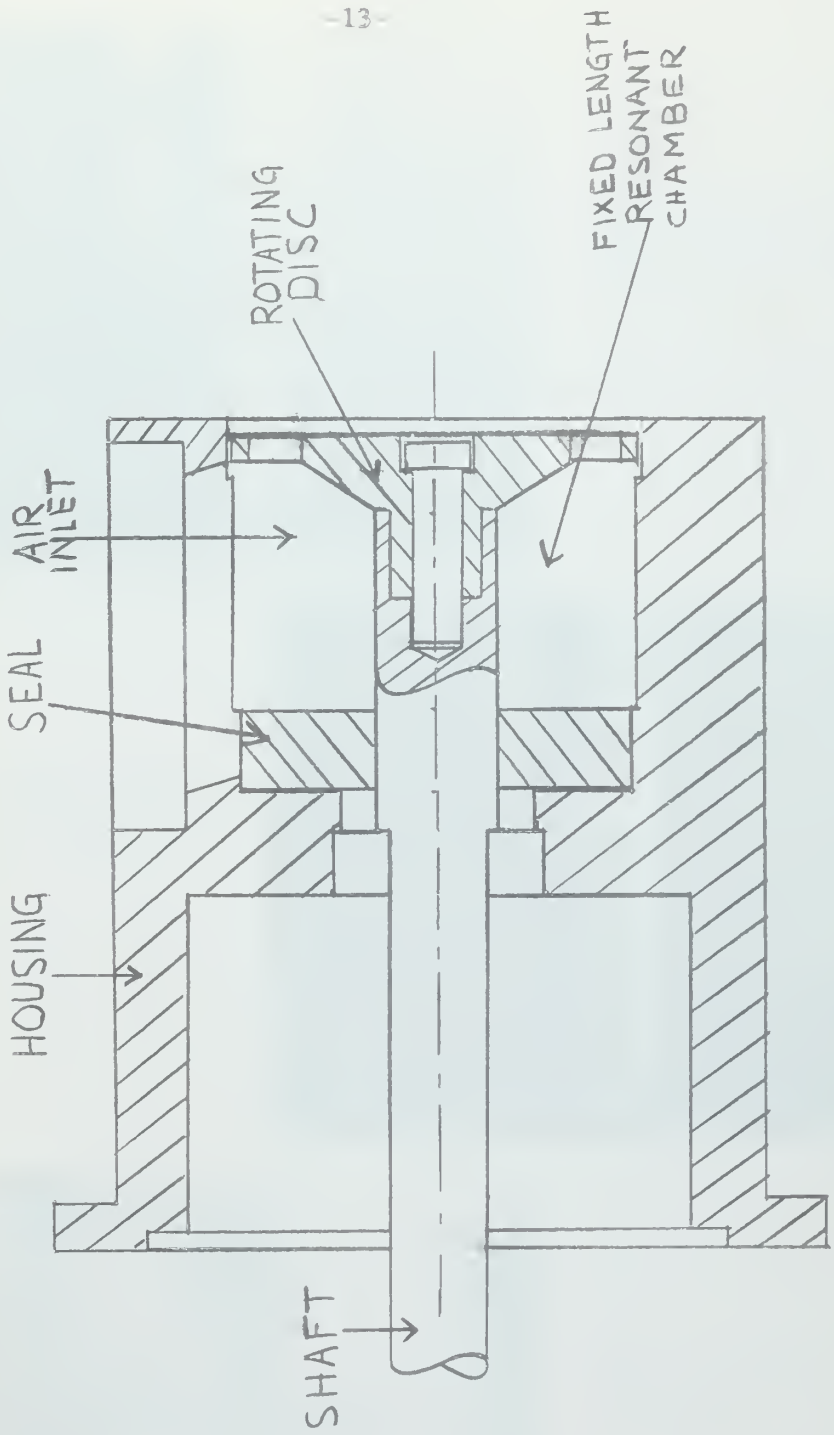

FIGURE 2 CROSS-SECTION OF ORIGINAL SIREN

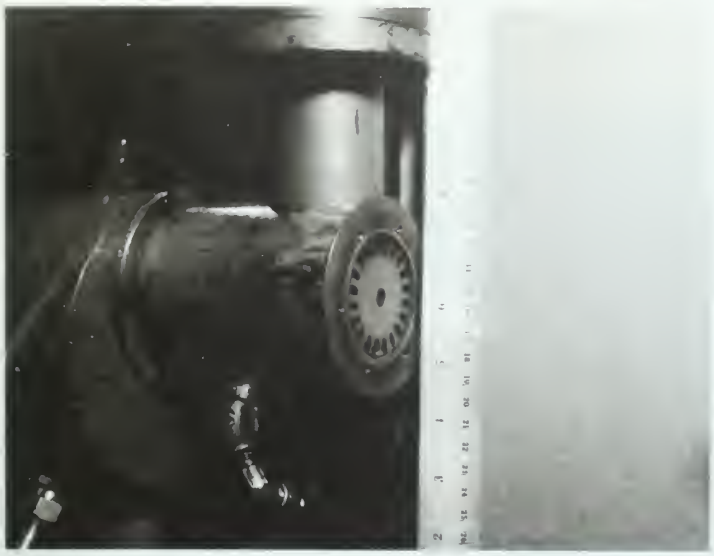

Figure 3a. Siren showing rotating disc with the stationary disc removed

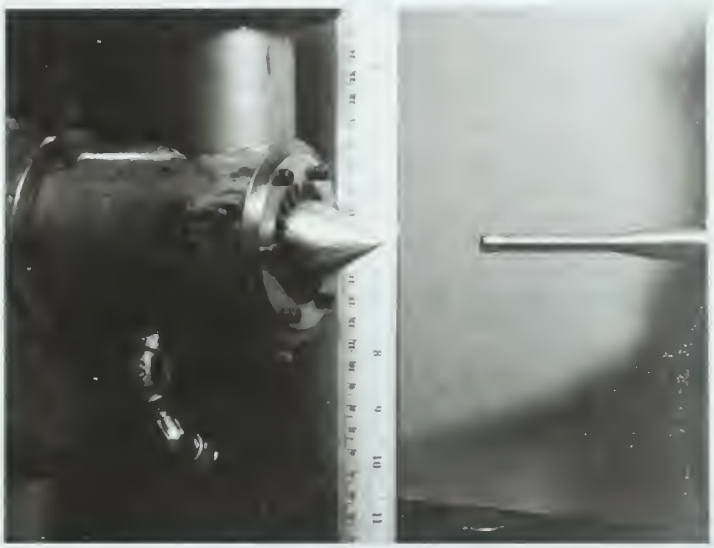

Figure 3b. Siren showing stationary disc and the microphone

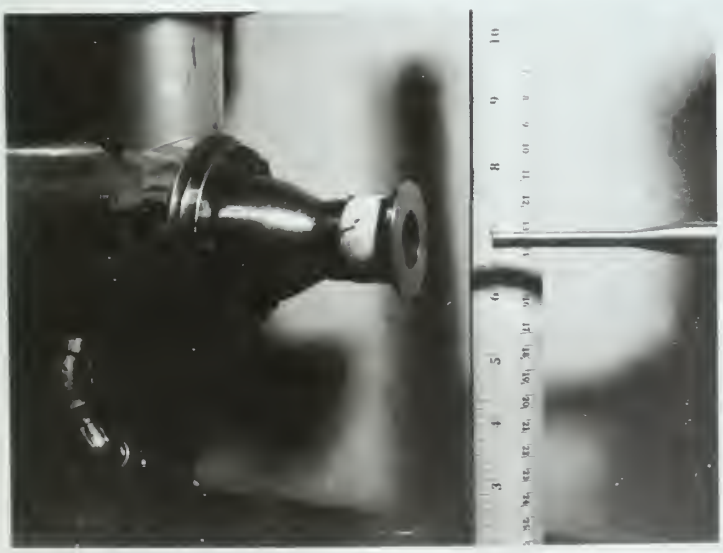

Figure 3c. Siren showing the nozzle and the microphone

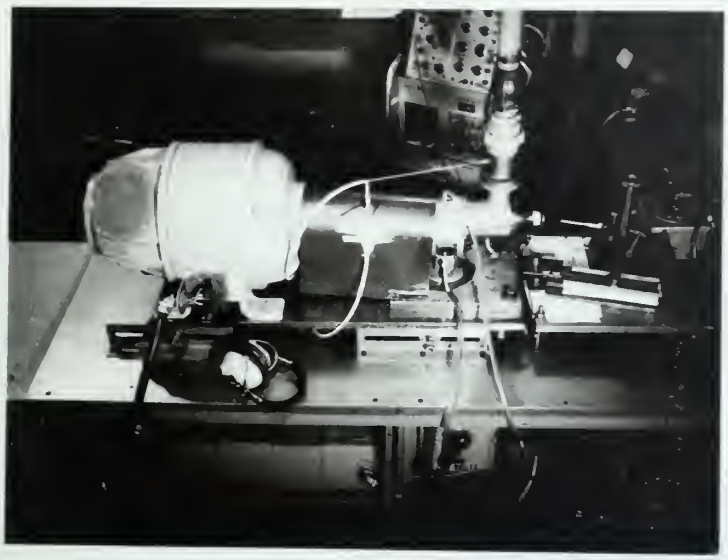

Figure 4. Complete siren showing the microphone in position

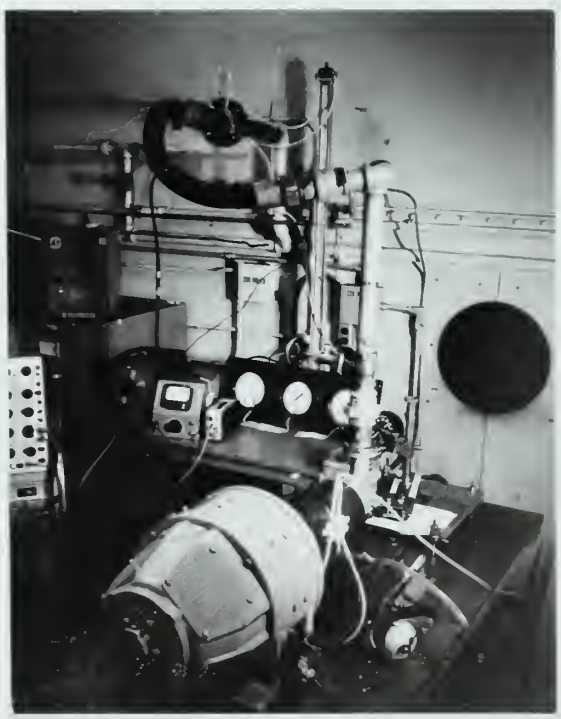

Figure 5. Complete siren showing the instrumentation and the test apparatus

PROCEDURE

The scheme for achieving the end result of an improved air chopper which would be more likely to break test specimens at the higher frequencies consisted of four steps. First, the output from the existing chopper was measured carefully at various frequencies and two configurations. Second, changes to the chopper were proposed on the basis of conclusions drawn from the results of Step One. Third, the chopper was retested in its new form to see how the output had changed and to find new capabilities. Fourth, the results of Step Three were compared with Step One to see if there had been a change in the chopper's output. The comparison of Step One and Step Three takes place in the Discussion of Results section.

Before experimenting could begin, a major problem was to find a pressure transducer or microphone which could accurately measure the chopper's output. It was known that the output would be of very high intensity and, of course, the frequency range was up to 15,000 cps. The combination of high frequency and high intensity level severely limited the number of possible devices which could be used. The Bruel and Kjaer ½" (type 4135) condenser microphone was finally chosen. This, in conjunction with the B. & K. type 2615 cathode follower and type 2801 power supply, provided sound intensity (SPL) measurements in units of decibels. The microphone and accessories are shown in Figure 4. The microphone can stand intensities up to 180 db and has an essentially constant output at all frequencies up to 40,000 cps. The output was read on a Ballantine RMS voltmeter.

A Ballantine Peak-to-Peak voltmeter was connected in parallel with the RMS voltmeter for safety's sake, to be sure that peak output values never exceeded the 180 db which would damage the microphone.

It would have been desirable if the microphone could have been placed at the air exit plane of the chopper. In that manner the chopper's output could have been measured at the location where it would be applied to gas turbine blades under test. This was not possible, however, because the sound intensities at this location exceed the 180 db limit imposed by the B. & K. ¼" microphone. In fact, to be certain that the diaphragm of the microphone would not fracture, and also to stay within the linear range of its cathode follower, it was desired to limit the microphone's exposure to sound fields of 170 db or less. This meant that the microphone had to be placed at a distance from the chopper's air exit plane and away from its perpendicular axis.

For the experiments conducted to determine the chopper's output, the microphone was used to measure the acoustic field strength at various frequencies and configurations. This was done to obtain actual radiation patterns for comparison with predicted patterns, and also to obtain the power out of the chopper.

Predicted output radiation patterns were obtained by treating the chopper as a "ring source" of sound. Using this treatment, and measured values of the mass flow rate of air through the chopper, it was possible to predict the sonic intensity at any location relative to the source. The "ring source" development is shown in

Appendix C. Thus, the predicted source strength and lobing effect enabled one to see how SPL would change with different angles from the axis. Further, values of SPL could be estimated at locations where the intensity was too high to be safely measured by the B. & K. microphone.

The power out of the chopper could have been best obtained by integrating a series of intensity (watt/m^2) readings taken in the air exit plane. Intensity could not be measured in the air exit plane without damage to the microphone. Therefore, measurements were made at a constant radius and at various angles away from the chopper's axis. By assuming a symmetrical directivity pattern of sound, the intensities at constant radius and 10^o increments from 0^o to 90^o were integrated numerically to obtain the power output of the chopper in watts. The intensity values at the 10^o increments were obtained from converted SPL readings. The method of integration is shown in Appendix D. Generally the SPL at 0^o was too high to be safely read with the B. & K. microphone. This was evident as the angle off the axis was slowly decreased from 10^o to 0^o and the voltmeter indicated a high rate of SPL increase above the value at 10^o. Therefore the SPL at 0^o was estimated from the predicted radiation patterns.

Step One -- Procedure for Testing the Original Air Chopper

The experimental set-up for conducting Step One is as shown in Figures 5 and 6. All of the equipment was located in a test cell in an isolated storage building at General Electric's West Lynn plant,

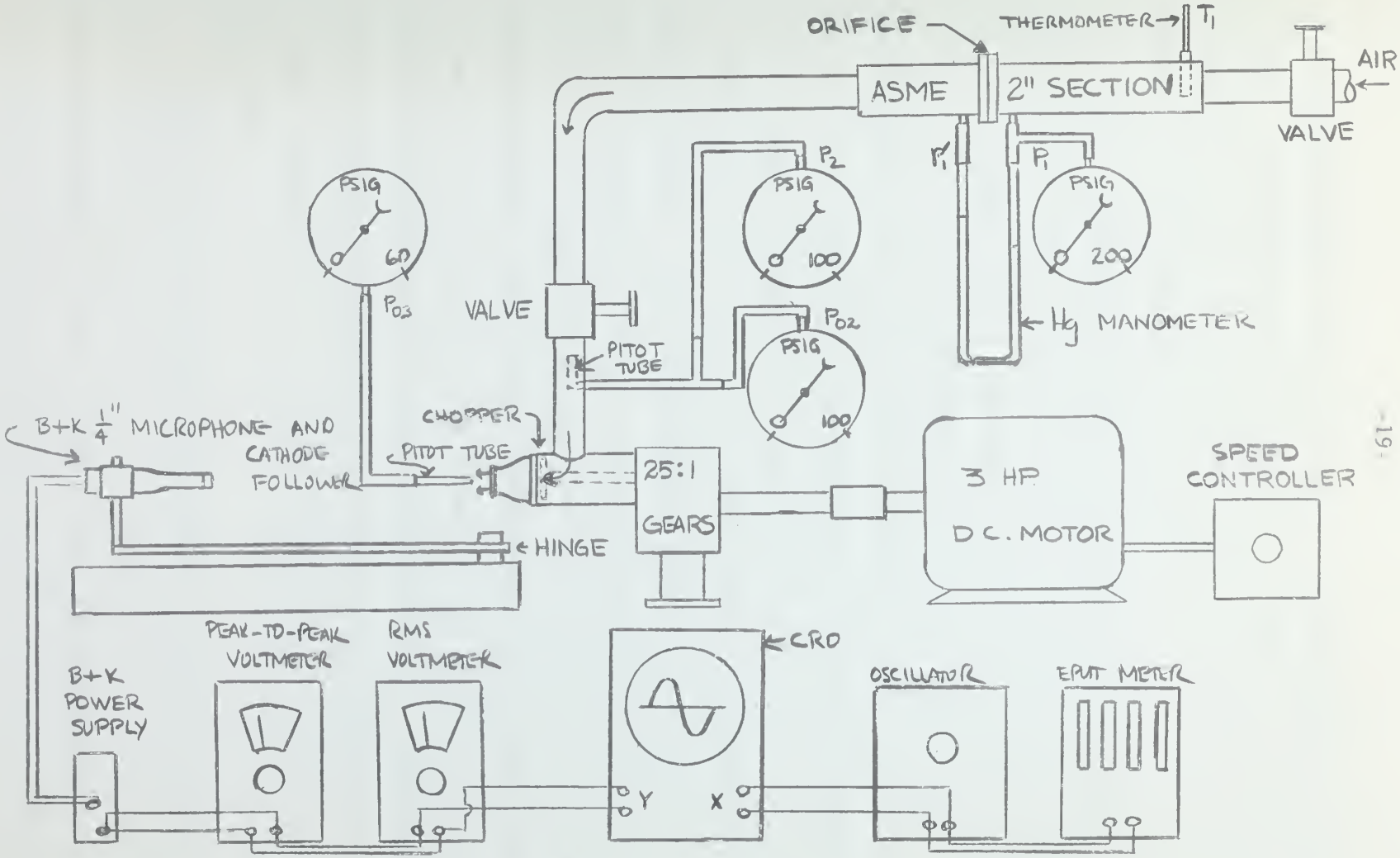

Figure 6. Schematic of Experimental Apparatus

so no special methods were used to muffle the sonic output of the chopper. Consequently, when operating the chopper, it is necessary to protect one's ears by wearing ear plugs and ear covers. Communication was by prearranged visual signal.

Air at approximately 100 psi is provided to the test cell, and this is the chopper's source of air power. Upstream of the chopper, in the air supply line, a flow meter consisting of an ASME standard 2" test section and a square-edged orifice was installed (10) Pressure difference across the orifice was measured with a mercury manometer and air temperature was measured with a thermometer upstream at the proper (ASME specified) distance from the orifice. Pressure pickup points in the test section were located in accordance with ASME directions. Static and stagnation pressure were read with a pitot tube inserted in the air supply just upstream of the siren chamber. Air temperature at this point was assumed to be the same as that measured in the ASME test section farther upstream (since it was not very far removed from it and, in any case, the air temperature was never very far above room temperature). Stagnation pressure was also measured in the airstream at the chopper exit using a probe. The method of calculating flow rate, w_t, is given in Appendix A.

Sound pressure level (SPL) measurements were made using the Bruel and Kjaer ½" microphone previously described. A rigid mount for the microphone, shown in Figure 4, was used which would permit positioning it at desired directions (from 0^o to 90^o) and distances

(0 to 32 cm) from the chopper exit plane. The microphone was insulated from high frequency vibrations by wrapping it in 3/32" rubber sheeting prior to attaching it to the mount.

Microphone output (SPL) was read in volts on the Ballantine RMS voltmeter. The voltage readings (v) were converted to RMS decibels using the calibration data given with the microphone:

-73.4 db re 1v/ubar.

$$\text{SPL (re 0.0002 ubar)} = 74 + 73.4 + 20 \log_{10} v. \qquad (1)$$

In addition, the microphone output waveform was observed on a Tektronix oscilloscope fitted with a Polaroid scope camera. This provided the waveform pictures in Figures 8-12, (b) and (c). The oscilloscope also provided the means for accurately measuring the output frequency of the chopper. A signal of controllable frequency was fed into the oscilloscope "x" input from an oscillator. The amplified microphone signal was fed into the "y" input of the oscilloscope and its frequency could be matched by varying the oscillator frequency until the proper elliptical lissajous figure came into view on the scope screen. At that point the frequency indicated on the oscillator is the frequency of the chopper. Since the oscillator's output was measured by an EPUT meter, the chopper's exact frequency at any speed could be obtained within one cycle per second.

Air supply pressure to the chopper could be controlled by the two valves in the supply line. It became evident, however, that the higher the pressure the more intense the chopper's output. After some initial experimenting it was decided to run the chopper with the

valves completely open, since maximum possible intensity was the goal.

The mass flow rate is an important parameter in calculating the acoustic field strength of the siren. It was measured whenever other readings were taken. However, the entire mass flow rate, w_t, does not contribute to sonic output. There is an unavoidable amount of leakage through the space between the rotating disc and the chamber wall, and also between the rotating and fixed discs. This leakage flow contributes nothing to the acoustic output since it is not chopped. Therefore, the total mass flow rate, measured with the flow meter upstream of the chopper, consists of a useful part (that is chopped) and a part wasted in leakage. It was necessary, then, to measure the leakage flow rate, and subtract it from the measured flow to obtain a "corrected" flow rate which could be used to obtain predicted sonic output values.

The leakage flow rate was measured when the chopper was stopped. The ports in the fixed and moving discs were aligned so that they were exactly out of correspondence, the situation which would ideally allow no flow whatsoever. In this condition the air supply valves were opened wide and the air flow, due entirely to leakage, was measured with the flow meter. It was found that a leakage flow of 0.175 lb_m/sec existed.

The chopper's output frequency was, of course, varied by changing the speed of the moving disc. The disc's speed was accurately controllable, and once set, remained very stable because of the 3 hp General Electric "Thymotrol" controlled motor driving it.

For Step One, the measurement of the output of the original air chopper, it was operated at frequencies in the range of about 7,000 to 15,000 cps. Lower frequencies were ignored because the chopper performs its intended task satisfactorily below about 7,500 cps. (This results from the smaller amount of energy required to excite blades in lower modes of vibration as indicated in the Introduction). The chopper's output at 15,000 cps. was particularly interesting, not only because it is the upper limit of its operation, but because occasions have arisen when it was desirable to fatigue test gas turbine blades in the vicinity of that frequency. Such fatigue tests have never been successful with the original form of the chopper. Further, the first tests were made with the nozzle, shown in Figure 3(c), in place since this was the "design" configuration for the chopper.

For all output sound pressure level measurements, readings were taken with the microphone positioned at two radii and 10° increments from 10° (0° was too intense for the microphone, as mentioned earlier) to 90° from the chopper's axis. An inner (closer) radius of 16 cm from the chopper air exit plane was chosen. At this radius no SPL greater than 170 db was found and, thus, it was a minimum "safe" distance from the chopper to insure protection of the microphone. Similar 10° increment readings were taken on a radius of 32 cm. This latter radius was chosen so readings at each angle could be compared with readings at the same angle at 16 cm radius. Since the distance from the sound source was doubled, it was expected that a 6 db lower reading at the greater distance at each angle would result, as predicted by the assumption of ideal spherical spreading.

With the "nozzle" in place readings were taken at 15,095, 12,347, and 8440 cps. The results of these readings are plotted in Figures 8(a), 9(a) and 10(a), along with their predicted values. Also, waveforms at angles of 20°, 50°, and 80° at both 16 cm and 32 cm at these frequencies are shown in Figures 8(b), (c); 9(b), (c); 10(b), (c). The first frequency, 15,095 cps, was chosen, as explained above, because it was the most interesting to us as the upper limit of the chopper (corresponding to maximum speed of the moving disc). As the frequency was lowered from the vicinity of 15,000 cps, a peculiar phenomenon was observed. Instead of smooth changes (either up or down) in output level, sharp peaks, or resonances, were noted as frequency was varied, and two of the strongest were at 12,347 and 8440 cps. A plot of sound pressure level versus frequency is shown in Figure 7. The resonant frequencies seemed to be of greater significance than the non-resonant frequencies. Therefore measurements to determine the radiation patterns were made at two resonant frequencies, 8440 and 12,347 cps. Note that at these resonant frequencies the SPL values are overall markedly higher than at 15,095 cps, a "non-resonant" frequency.

As stated in the Introduction, efficiency may be increased with a properly designed horn to expand the air from the ports smoothly. The "nozzle" on the chopper is an improperly designed horn and, intuitively, it was felt that the chopper might give higher output levels without it. Furthermore, the outlet area at the "nozzle" is smaller than the total port area, causing a restriction in mass flow rate. Therefore it was decided to run tests on the chopper

with everything identical to the previous tests but this time without the "nozzle." The chopper then appeared as indicated in Figure 3(b).

The first readings in the "no-nozzle" configuration were taken at 15,170 cps, again the top frequency available with the driving motor at full speed. Readings, waveform pictures, and data were taken exactly as before. The results at this frequency are shown in Figures 12(a), (b), and (c). Note that the SPL readings are higher than with the nozzle in place. Also the mass flow rate is higher, as predicted. Again, as the chopper speed was lowered following the investigation at the highest frequency, resonances were found. A particularly prominent resonance was located at 7,220 cps. This frequency was chosen to measure the chopper's output in a resonant condition. The results at this frequency are shown in Figures 11(a), (b) and (c). Note that these are the highest SPL's measured. Both the pronounced effect of resonance and the overall improvement of removing the nozzle are extremely well illustrated. From the point of view of treating the chopper as a siren, or sonic source, the "design" nozzle is obviously deterimental. It should be born in mind, however, that the chopper was designed for the specific purpose of concentrating its output on a gas turbine blade to fatigue test it. While this nozzle is obviously not the best one for the job, a properly designed nozzle could conceivably contribute to the chopper's effectiveness as a fatigue-tester. This remains to be shown.

Step Two -- Preliminary Results and Recommended Changes

A complete discussion of the results of the experiments performed

in Step One will be made in the Discussion of Results section later. Sufficient remarks on the results will be made here to justify the changes recommended.

The results of these initial experiments, shown in Table I and Figures 8-12, indicate that the chopper in its original form is an extremely powerful, if inefficient, noisemaker. The fact that it is a "brute force" siren, rather than one designed for high efficiency, was elaborated upon in the Introduction. The low efficiency, defined in Appendix B, did not matter particularly since a large source of "air power", also defined in Appendix B, is available. The principal aim, then, is to produce a louder siren (more effective chopper, presumably). Since the full air power available is used when running the chopper, increased output level will raise the efficiency, but never to the level of the most efficient possible sirens of this size (which use an overpressure of only an atmosphere or less in their chambers and consequently are not so loud). The results of the experiments of Step One suggest an obvious method to markedly increase the chopper's output: take advantage of resonance. At resonant conditions output power and efficiency were at least three times that at non-resonant conditions.

Other means of possibly improving the chopper's design were enumerated in the Introduction. Parameters like port size and shape, addition of a properly designed horn, etc., could be changed. However, the increased output resulting from these changes would probably not be large. The chopper had a high output power even in its original configuration, indicating that the design was very nearly as good

as could be expected for a siren that is restricted to such small dimensions.

Thus, the best means for increasing the chopper's output by a quantum leap was to take advantage of the resonance effect which had shown itself to be so powerful. The air chamber inside the chopper and upstream of the discs was modeled as an organ pipe, closed at one end and excited at the other, open end. If the length of the "pipe" is an odd integral number of quarter wavelengths, resonance occurs (9). By controlling the length of the chamber so that it is always one quarter wavelength long for the frequency at which the chopper is operated, it should be possible to force a resonance in the chopper.

To accomplish this a new chamber and associated parts were designed, as shown in Figure 13. To make the modification as simple as possible the existing driving mechanism (motor, gearbox, drive shaft) was left intact and the new chamber was designed to be interchangeable with the old one. This made it possible to use the discs from the original chopper, as well. The important difference is that the new chamber can be "tuned" to resonance by rotating the annular sleeve, shown in Figure 13.

Step Three -- Procedure for Testing the Modified Air Chopper

The new chamber design, shown in Figure 13, was intended to be the final output of this thesis: "An Improved Axial-Flow Siren for Fatigue Testing Gas Turbine Blades." It was designed so that its resonant frequencies could be controlled in the range from 7,000 to

20,000 cps. Thus, the chopper could be run at, and tuned to resonance to match, a desired turbine blade resonant frequency for fatigue testing.

Since the parts comprising this new chamber design are expensive to build, it was decided to simulate the effect of the new chamber design in a simple and cheap way to further insure that it is the best way to improve the air chopper.

To substantiate the contention that the dimensions of the chamber are the primary factors controlling resonant frequency it was decided to modify the length and radial dimensions to see if this does, in fact, change the chopper's resonant frequencies.

First, to change the length, a slug, one-half inch thick, shown in Figure 14(a), was installed at the rear of the original chopper's chamber, thereby decreasing its length. As explained in the Discussion of Results section, a shorter chamber should have resonances at higher frequencies.

To illustrate the effect of changing the length of the chamber, the speed of the siren was varied to correspond to the frequency range from 3,000 to 15,000 cps. Readings were taken at each 1,000 cps increment, starting at 3,000 cps, and also at the foot and peak of each resonance spike. The microphone was fixed at 20 cm distance and 15^{o} off the axis to measure the main lobe, but remain out of the air stream. The air flow through the siren was controlled so that it would be the same as that when the siren was run without the slug in the chamber (Figure 7). The resulting plot of sound pressure level

versus frequency is shown in Figure 15(b).

Once the length was changed, it was desired to further modify the chamber's dimensions so that it would resemble a "closed tube" or "organ pipe." This was used as the model for the resonance chamber in the improved version of the air chopper. The chamber was further modified by replacing the previous slug with another shaped as shown in Figure 14(b). Note that the resulting chamber with the new slug in place is quite similar to the resonating chamber in the improved version of the air chopper, Figure 13. The only difference is that the length of the chamber is not adjustable when the slug is used.

The effect on resonant frequencies of this second chamber modification was shown by taking sound pressure level readings in the range from 3,000 to 15,000 cps, as before. Sound pressure level versus frequency for this configuration is plotted in Figure 15(c).

The improved version of the air chopper, Figure 13, was not available in time to be tested.

RESULTS

The results stated below are divided into two categories: those derived from experiments with the original air chopper and those from the experiments with the modified version.

Original Air Chopper:

1. As indicated in the radiation patterns of Figures 8(a) - 12(a), this is a high intensity siren.

2. With mass flow rate constant, and at a given microphone position, frequency was varied to observe changes in intensity. Instead of varying smoothly as frequency was changed in the range of 3,000 to 15,000 cps, spikes of unpredictably high intensity were observed at particular frequencies. See Figure 7.

3. At 12,347 and 15,095 cps observed radiation patterns agreed quite closely with patterns predicted from the ring source model (see Figures 9(a) and 10(a)). At 15,170 cps observed and predicted patterns agreed substantially (see Figure 12(a)), while at 7,220 and 8,440 cps there was much less agreement (see Figures 11(a) and 8(a)).

4. As shown in Figures 8(b), (c) to 12(b), (c), the siren output waveforms were not sinusoidal, but more nearly sawtooth shaped.

5. Assuming spherical spreading from the siren source, a 6 db per distance doubling loss was predicted. In general this was the observed result for the 7,220, 8,440, and 15,170 cps experiments, as shown in Figures 11(a), 8(a), and 12(a). Figures 9(a) and 10(a) show that at the 12,347 and 15,095 cps experiments the results do not

agree well with the 6 db loss per distance doubling predicted.

6. Referring to Table I:

a) Low efficiencies were observed at all frequencies.

b) The highest efficiencies were noted at frequencies where high intensity spikes occurred.

c) Efficiency was higher without the nozzle than with it installed.

d) Efficiency was higher, in general, when calculations were based on data taken at 32 cm from the siren than when the data at 16 cm were used.

Modified Air Chopper:

1. The resonances observed with the two chamber modifications and those observed with the original chamber occurred at different frequencies. The results of these observations are shown as Figures 15 and 16.

2. As shown in Figure 15, in general, the chopper output intensity level is higher at lower frequencies.

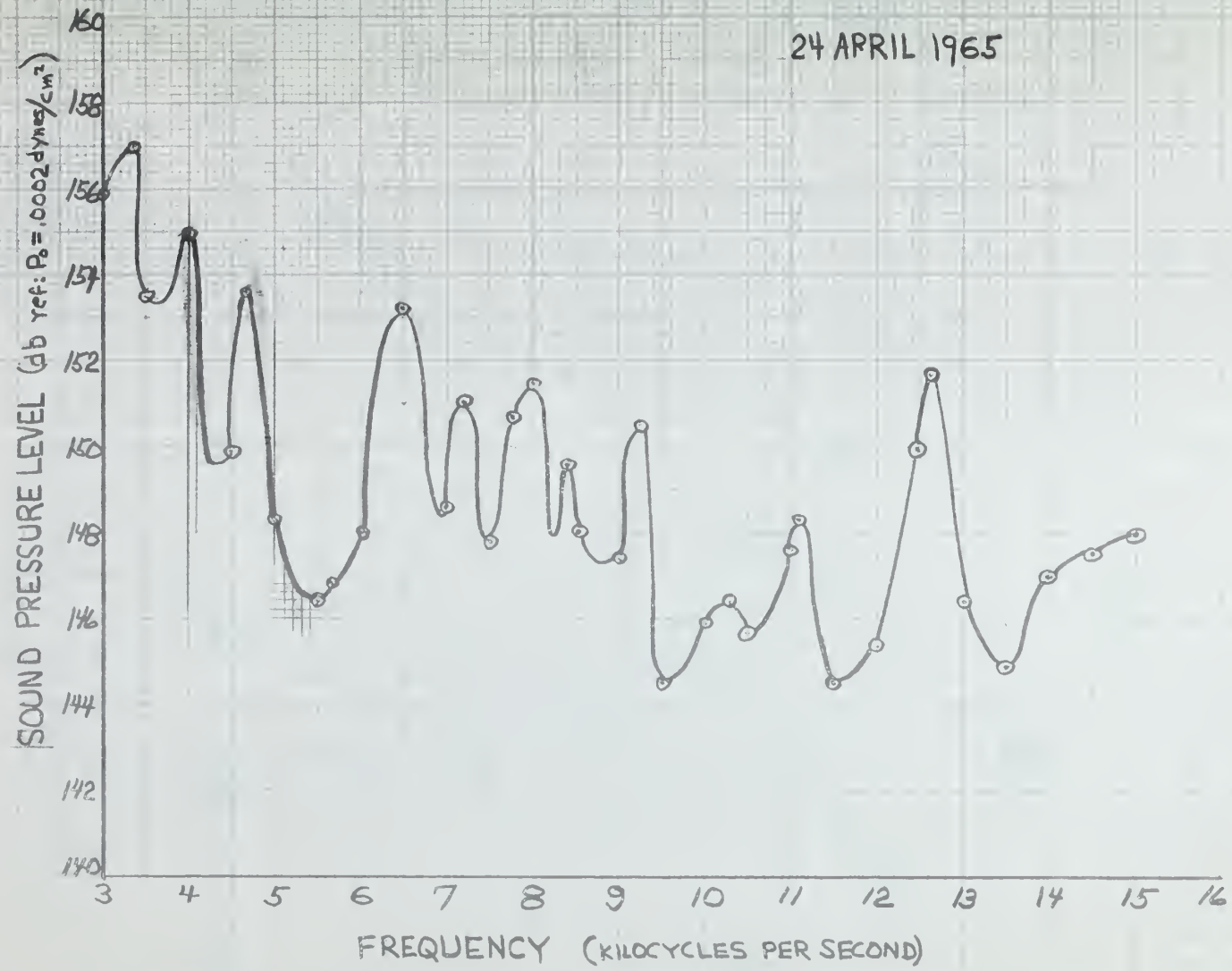

FIGURE 7 SOUND PRESSURE LEVEL vs FREQUENCY FOR ORIGINAL SIREN

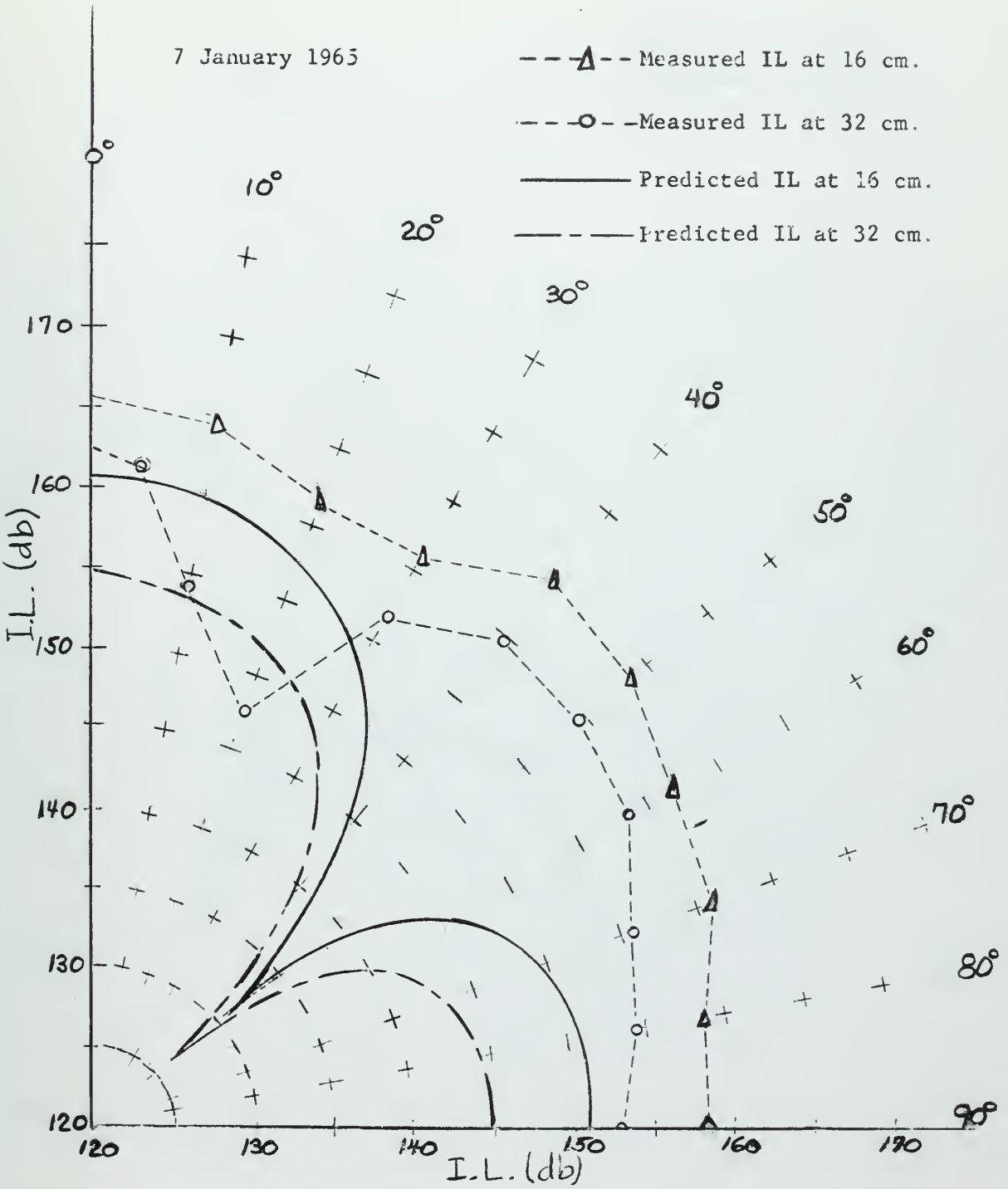

Fig. 8(a) Polar Radiation Patterns for Pulsed-Air Vibration Tester operated at 8440 c.p.s. with mass flow rate equal to 0.508 pounds per second. Nozzle Installed. IL = Intensity Level = 10 Log I/I_o; $I_o = 10^{-12}$ watts/meter^2.

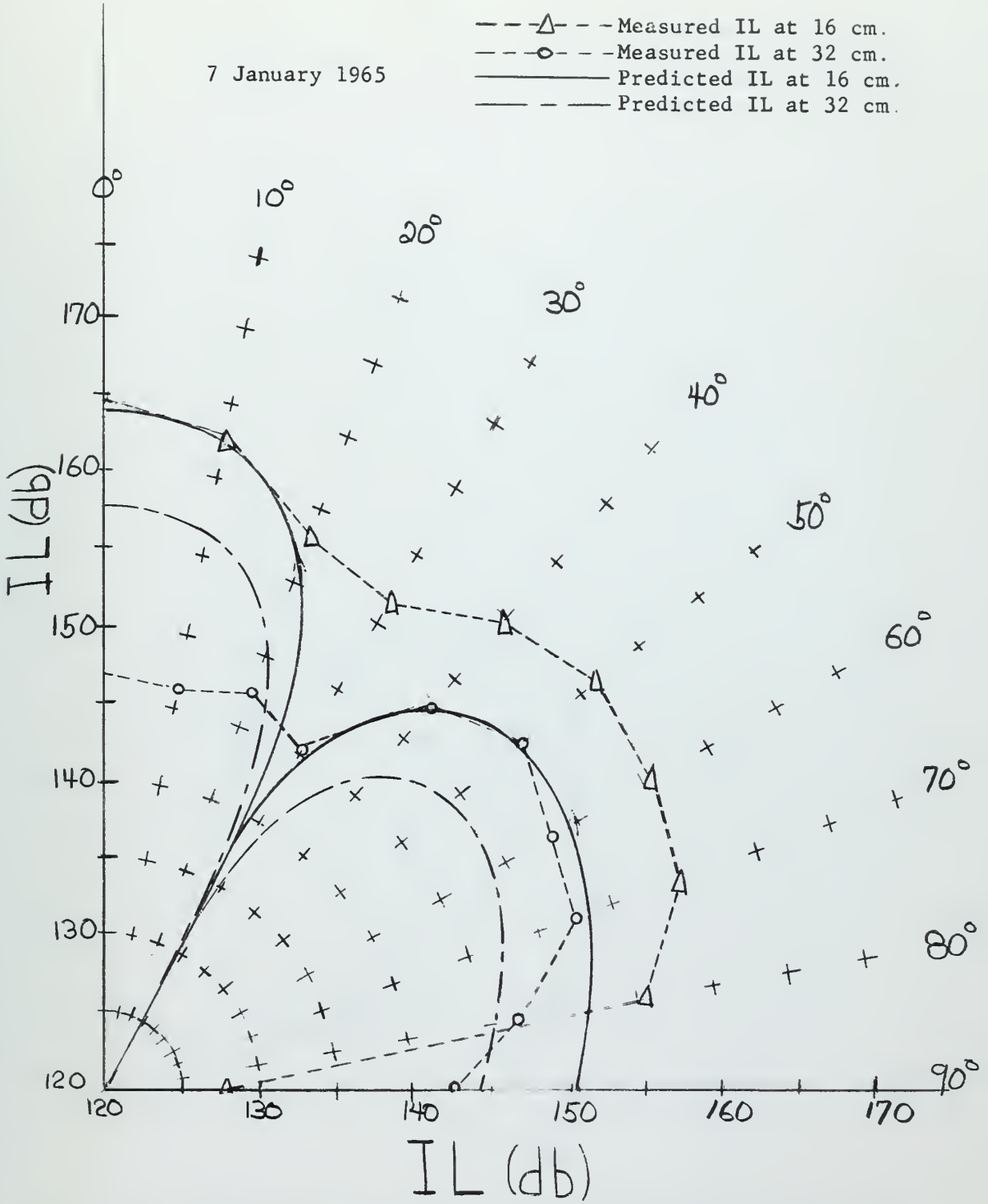

Fig. 9(a) Polar Radiation Patterns for Pulsed-Air Vibration Tester operated at 12,347 c.p.s. with mass flow equal to 0.52 pounds per second. Nozzle Installed

IL = Intensity Level = 10 Log I/I_o $I_o = 10^{-12}$ watts/meter^2

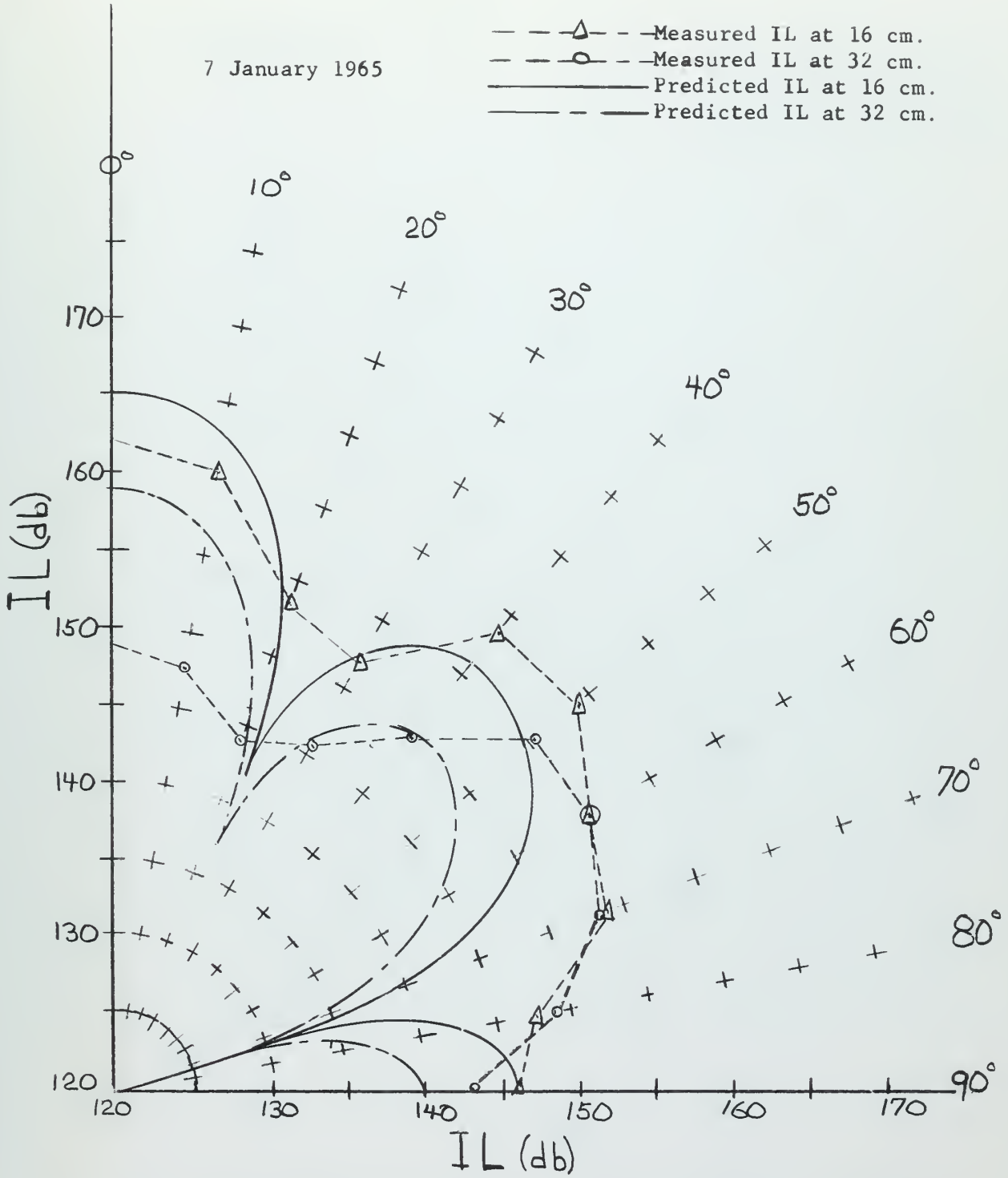

Fig. 10(a) Polar Radiation Patterns for Pulsed-Air Vibration Tester operated at 15,095 c.p.s. with mass flow rate equal to 0.508 pounds per second. Nozzle installed.

IL = Intensity Level = 10 Log I/I_o; $I_o = 10^{-12}$ watts/meter^2

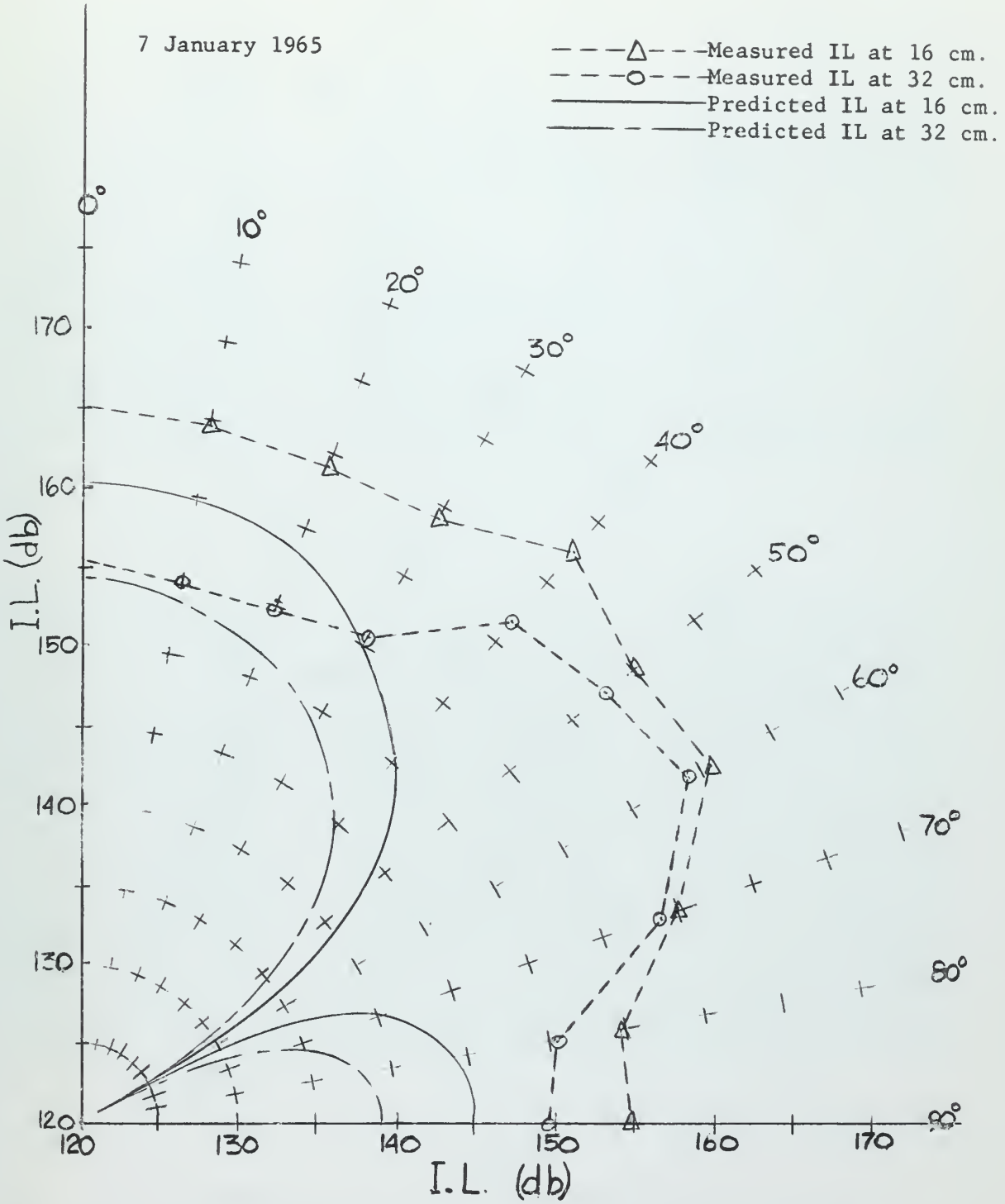

Fig. 11(a) Polar Radiation Pattern for Pulsed-Air Vibration Tester operated at 7220 c.p.s. with mass flow rate equal to 0.559 pounds per second. No nozzle installed.

IL = Intensity Level = 10 Log I/I_o; $I_o = 10^{-12}$ watts/meter^2.

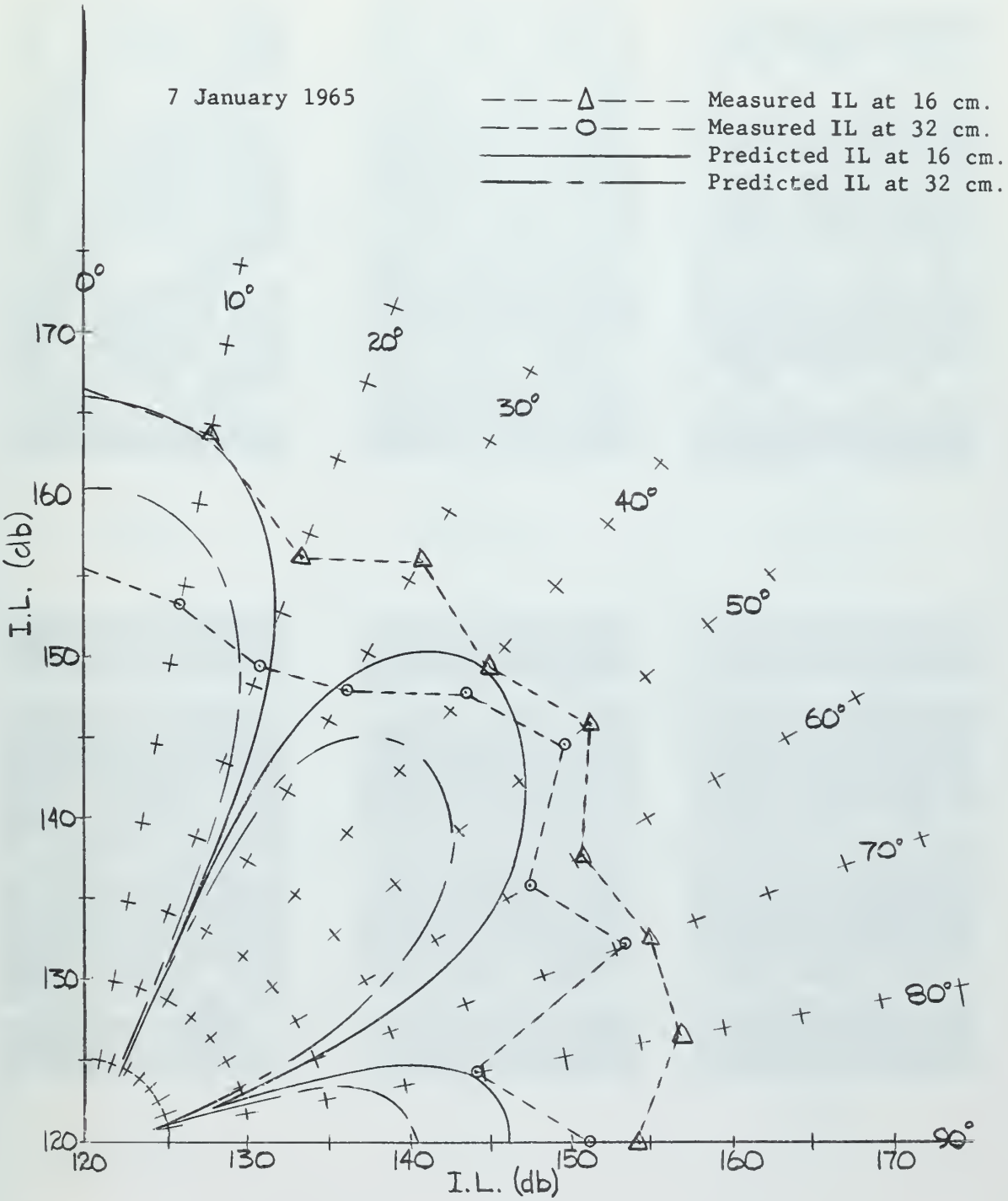

Fig. 12(a) Polar Radiation Patterns for Pulsed-Air Vibration Tester operated at 15,700 c.p.s. with mass flow rate equal to 0.553 pounds per second. No nozzle installed.

IL = Intensity Level = 10 Log I/I_o; $I_o = 10^{-12}$ watts/meter^2.

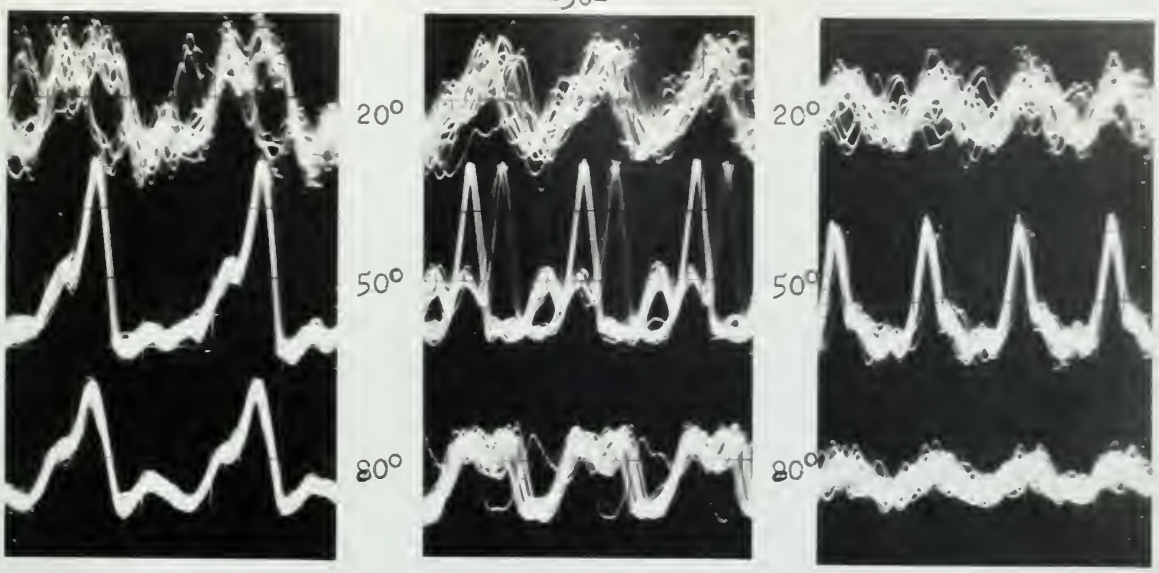

8(b)
8,440 cps
16 cm

9(b)
12,347 cps
16 cm

10(b)
15,095 cps
16 cm

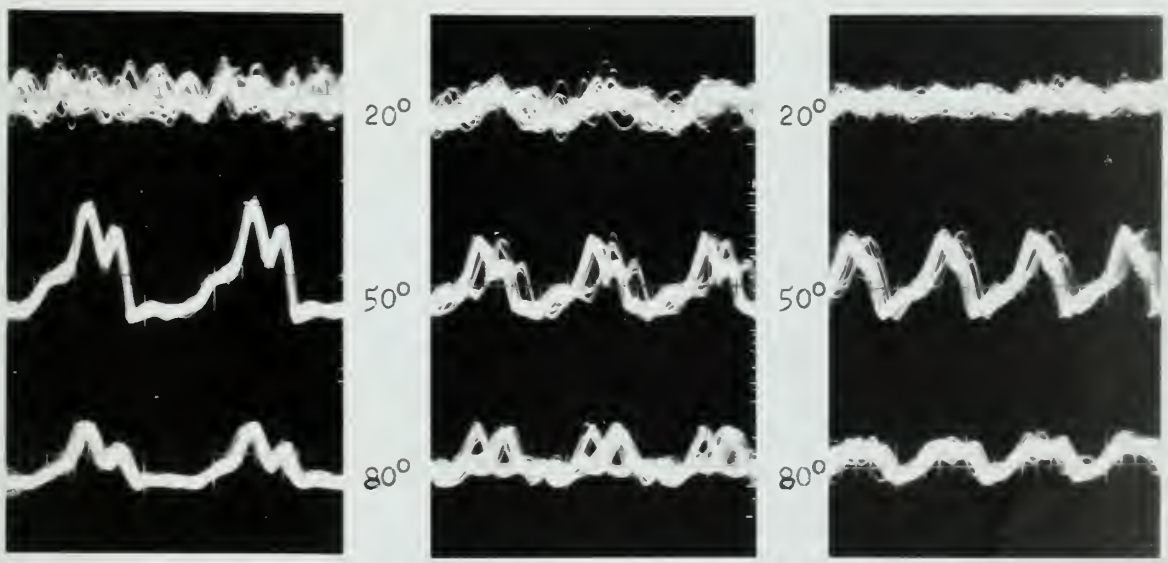

8(c)
8,440 cps
32 cm

9(c)
12,347 cps
32 cm

10(c)
15,095 cps
32 cm

Figures 8(b), (c) through 10(b), (c). Output waveforms from the Air Chopper with nozzle installed observed at 16 cm and 32 cm radii and 20°, 50°, and 80° from the axis.

11(b)
7,220 cps
16 cm

20°
50°
80°

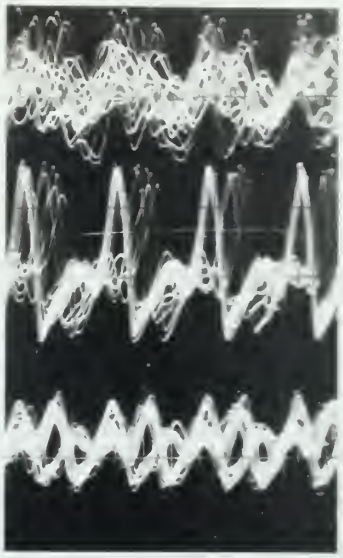

12(b)
15,170 cps
16 cm

11(c)
7,220 cps
32 cm

20°
50°
80°

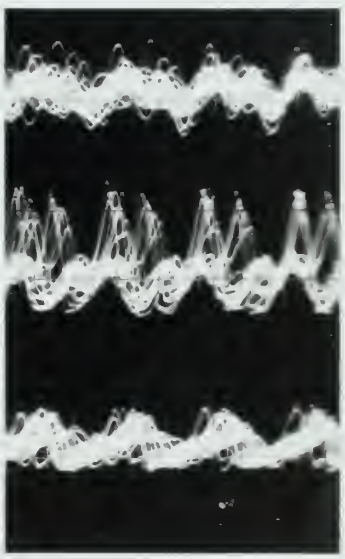

12(c)
15,170 cps
32 cm

Figures 11(b), (c) and 12(b), (c). Output waveforms from the Air Chopper without nozzle observed at 16 cm and 32 cm radii and 20°, 50°, and 80° from the axis.

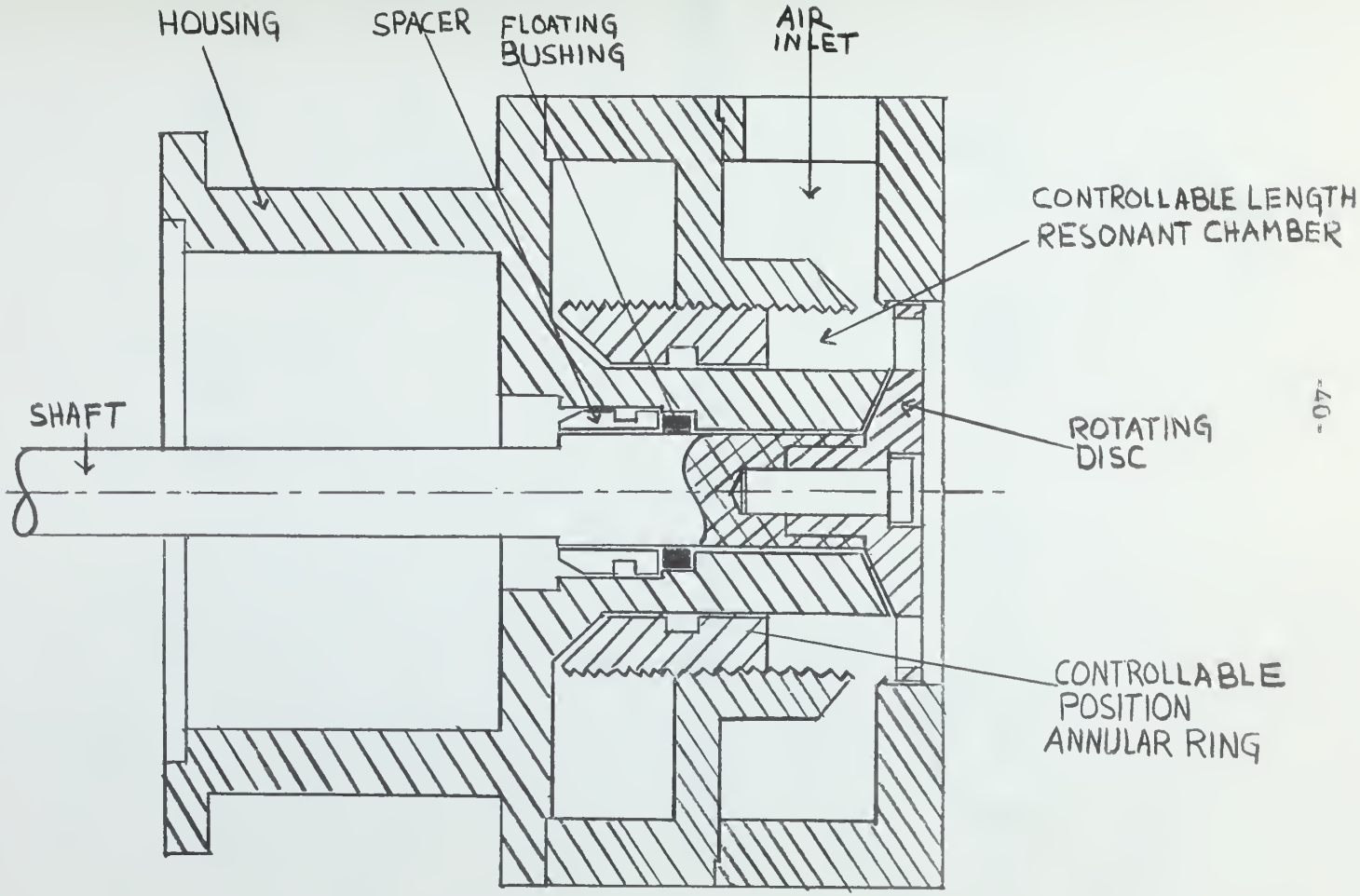

FIGURE 13 CROSS-SECTION OF MODIFIED SIREN

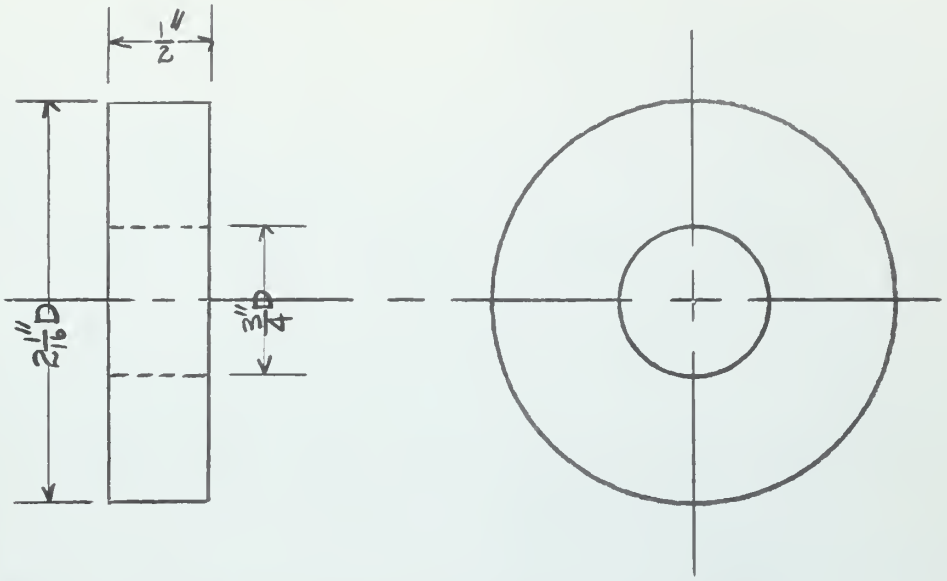

Figure 14(a). Plug for Modifying Chamber Length.

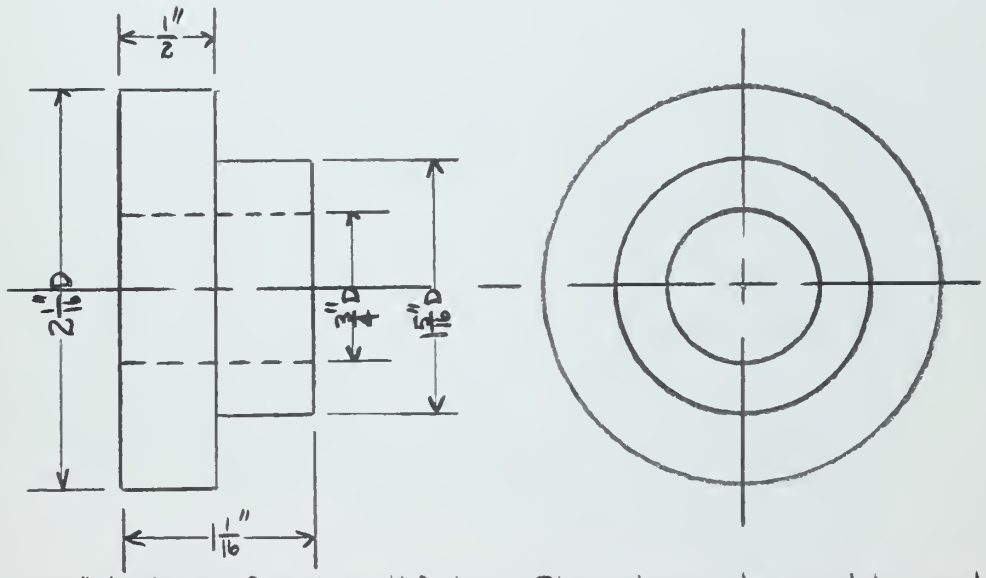

Figure 14(b). Plug for Modifying Chamber Length and Diameter.

Figure 14. Chamber Plugs.

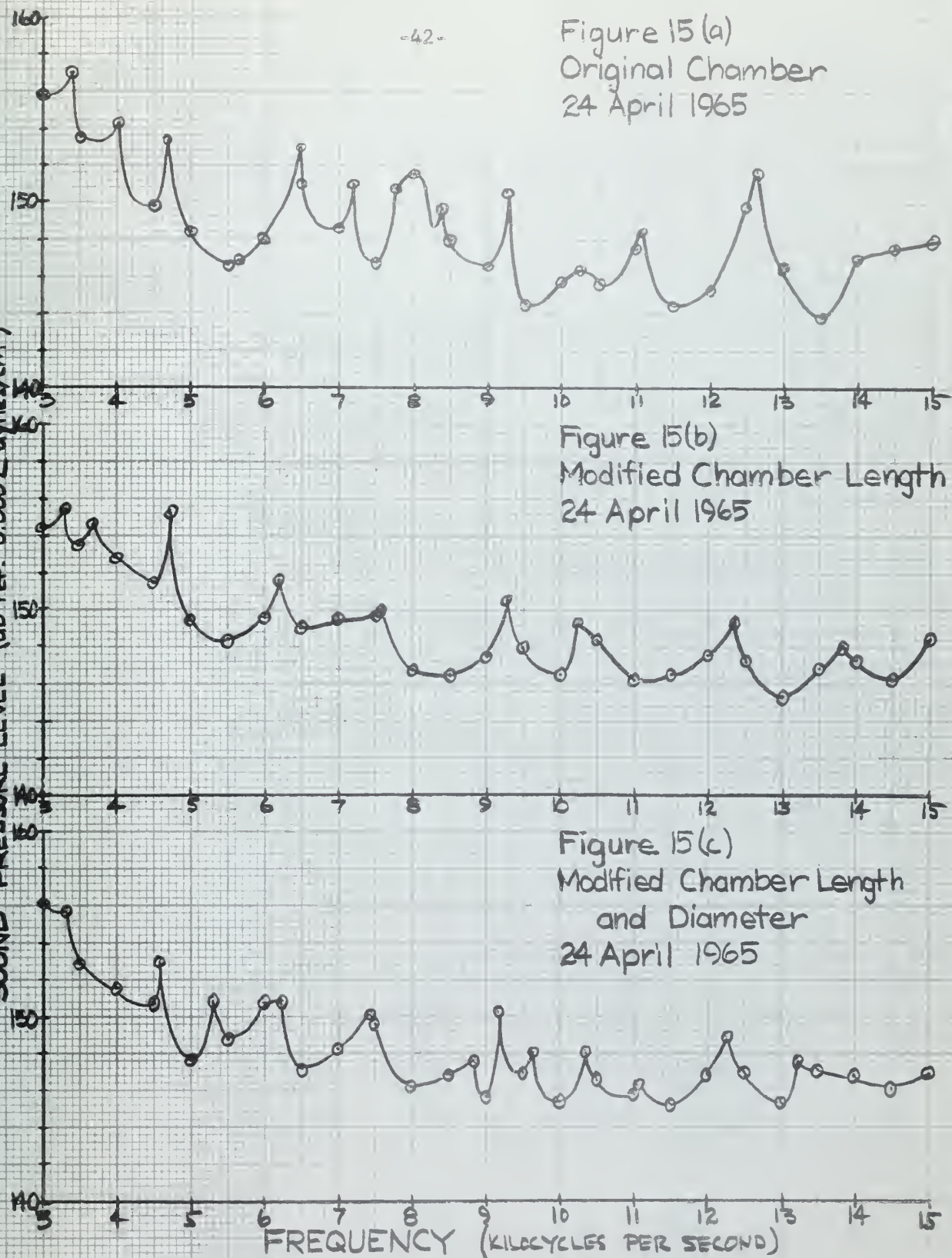

Figure 15. Sound Pressure Level vs. Frequency for Three Siren Chamber Configurations.

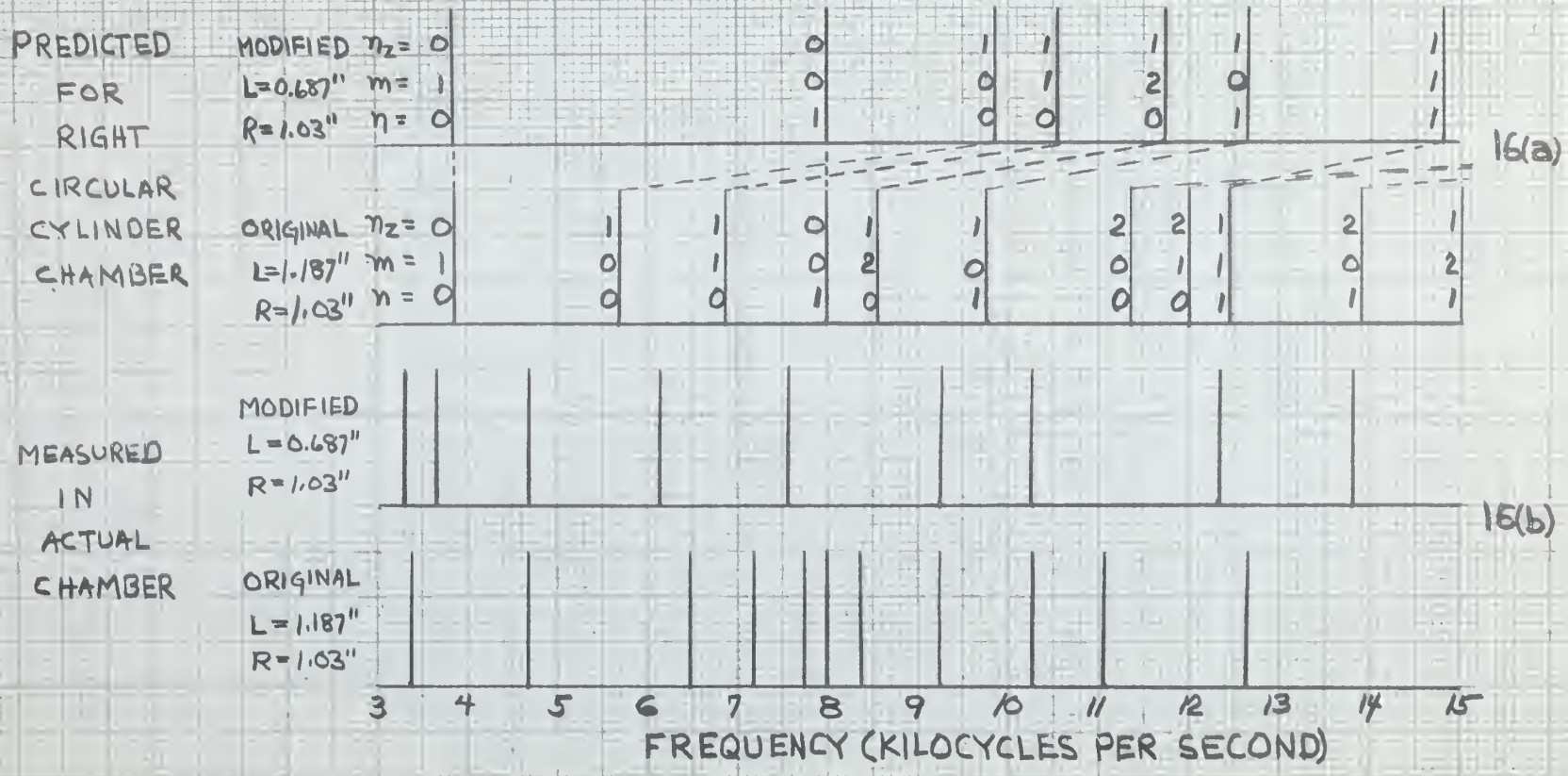

FIGURE 16 LOCATION OF NATURAL FREQUENCIES

TABLE I

Frequency (cps)	8,440	12,347	15,095	7,220	15,170
Resonant	Yes	Yes	No	Yes	No
Nozzle	Yes	Yes	Yes	No	No
Air Power Available (watts)	27,500	27,500	26,800	29,500	29,400
Microphone at 16 cm radius					
Acoustic Power Out (watts)	2,653	1,259	573	3,710	1,268
Efficiency	9.6%	4.6%	2.1%	12.6%	4.3%
Microphone at 32 cm radius					
Acoustic Power Out (watts)	3,177	974	1,091	6,419	1,696
Efficiency	11.6%	3.5%	4.1%	21.7%	5.8%

DISCUSSION OF RESULTS

Original Air Chopper:

1. High Intensity Siren.

The highest intensity reading was 167.5 db, at 16 cm and 40° off the axis, at 7,220 cps. For a rough cut, assuming spherical spreading (6 db per distance doubling), at 1 cm from the siren the intensity level should be 191.5 db, certainly a high intensity acoustic source.

2. Spikes of Unpredictably High Intensity.

The spikes of unpredictably high intensity which occurred at 7,220, 8,440 and 12,347 cps were assumed to be caused by resonances taking place within the siren apparatus. The nozzle was ruled out as a possible source since the resonances occurred with or without it. The cylindrical air chamber, shown in Figure 2, just upstream of the rotating disc, was the remaining obvious source of resonance. It was impossible to analyze it precisely, to correlate its dimensions with the wavelengths at various frequencies, because its irregular shape does not lend itself to exact mathematical treatment. Basically, however, the chamber is a right circular cylinder. The irregularities arise from the air supply line entering one side, the drive shaft running down its center, and the shape of the rotating disc at one end.

If the diameter of the chamber had been very small, say 0.1 wavelength, the chamber could have been modeled as a closed tube,

or "organ pipe." In fact, the dimensions of the improved version of the air chopper, described elsewhere in this thesis, permit this model to be used. Since the diameter of the chamber of the original air chopper is greater than one-half wavelength, however, it can be treated as a "small room" (2)

In a cylindrically shaped small room of length ℓ and radius a, the solution of the wave equation in cylindrical coordinates is (9):

$$P = \begin{matrix}\cos \\ \sin\end{matrix}(m\varphi)\cos\left(\frac{W_z z}{c}\right) J_m\left(\frac{W_r r}{c}\right) e^{-2\pi ft} \qquad (2)$$

where

$$f = \frac{1}{2\pi}\sqrt{W_z^2 + W_r^2}$$

c = velocity of sound in air

To have the z component of particle velocity zero at z = 0 and z = ℓ, $\frac{dp}{dz}$ must be zero at these points. The derivative is automatically zero at z = 0 since the function is cosine. For it to be zero at z = ℓ, $\frac{W_z \ell}{c} = n_z \pi$, ($n_z$ = 0,1,2 ...) must occur. To have the radial particle velocity zero at the cylinder walls, $\frac{dJ_m}{dr} = 0$ must occur at r = a. For this to be true, $\frac{W_r a}{c} = \pi \alpha_{mn}$ must occur, where α_{mn} is a solution of the equation $\frac{d}{d\alpha} J_m(\pi\alpha) = 0$. The characteristic functions for the cylindrical room are therefore those given in Equation 2, and the characteristic values are

$$W_z = \frac{\pi n_z c}{\ell} \qquad (n_z = 0, 1, 2 \ldots)$$

$$W_r = \frac{\pi \alpha_{mn} c}{a}$$

Therefore the natural frequencies for the small room are given by:

$$f = \frac{c}{2}\sqrt{\left(\frac{n_z}{\ell}\right)^2 + \left(\frac{\alpha_{mn}}{a}\right)^2} \qquad (3)$$

where values of α_{mn} can be obtained from Table 5 of Reference 9.

Equation (3), which permits an infinite number of solutions, coupled with the fact that the cylinder has irregularities, does not provide the desired exact numerical proof that the chamber causes resonance. However, for combinations of low values of n_z, m, and n, the predicted resonances are well within the range of the actual resonances. Figure 16(a) shows possible resonant frequencies for the dimensions of the original chopper.

The rear end of the cylindrical chamber is a perfectly flat surface. Waves are excited within the chamber by the air pulses occurring when the chopper ports open and close. These waves reflect, in phase, off the flat back wall of the chamber. Even though the chamber diameter is of the order of magnitude of a wavelength, it can be very roughly modeled as an organ pipe or closed tube to permit another estimate of its effect on resonance. Ignoring standing waves resulting from anything but its lengthwise dimension, then, it can be seen that the length coincides very nearly with small, odd integral numbers of quarter wavelengths. For instance, at 7,220 cps a quarter wavelength is 0.468 inch. Three quarter wavelengths at this frequency equal 1.4 inches, which is quite near the chamber length of 1.187 inches.

Lacking more precise calculation methods, this qualitative

approach well supports the contention that the chamber is the source of the resonances, or "spikes" in the air chopper.

There seemed to be no way to quantitatively account for the magnitude of the siren's output at resonance. Hence, even at resonant conditions, predicted radiation patterns were plotted using the calculation method of Appendix C. It was assumed that U_o was the same as, and could never be more than $\overline{U}_o$ as shown by curve (a) in Figure 17 and explained in the same appendix. This assumption was made because the calculated U_o was based on a one-way mass flow of air through the siren discs which could obviously never be negative. In fact, at non-resonant conditions, this assumption proved to be reasonable. It gave fairly good agreement between predicted and actual results, as shown in Figures 10(a) and 12(a).

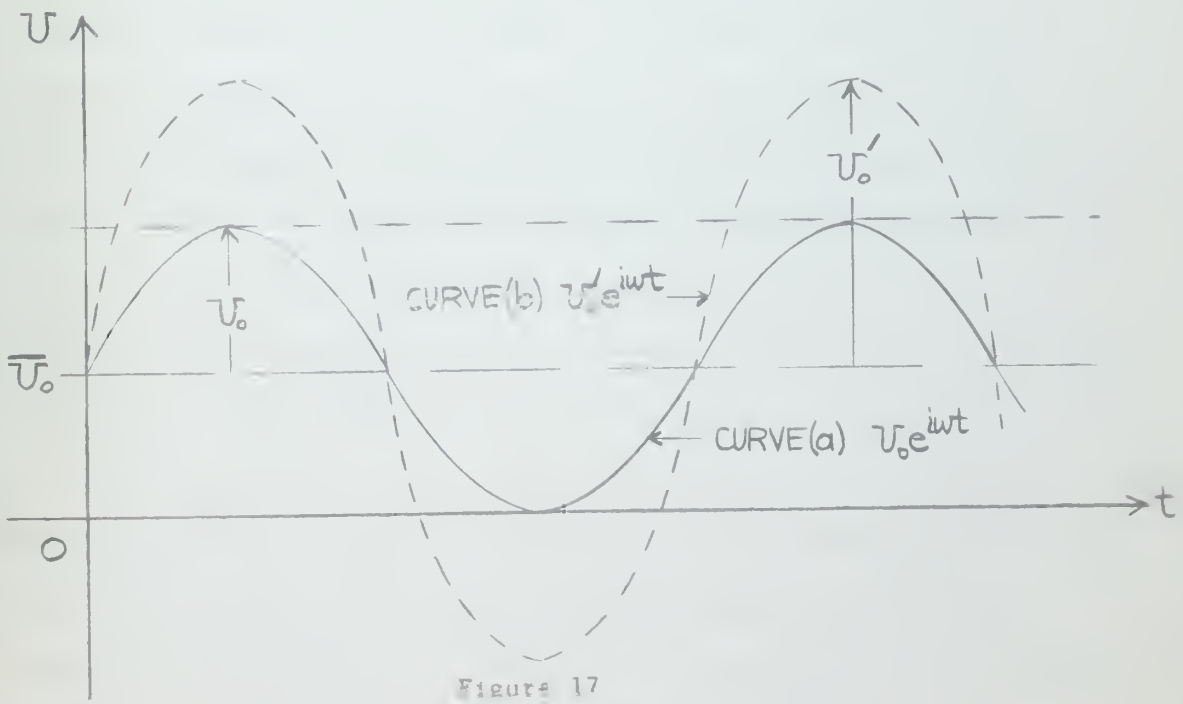

Figure 17

Air Piston Velocity

At resonant conditions average mass flow rate was shown to be virtually the same as at non-resonant conditions. Since the mass flow rate, the basis for predicting the chopper's output at non-resonant conditions, was the same, it was difficult to explain the increased output intensity. Certainly $\bar{U}_o$ was the same as at non-resonant conditions. The difference is that velocity amplitude, U_o, of each port or "air piston" must increase to a new value, U'_o, not limited by the fact that air flow through the siren ports is one-way only. Thus, at resonance, it must be assumed that even though $\bar{U}_o$ does not increase, the standing waves occurring in the air chamber greatly increase the air piston's velocity amplitude. As curve (b) in Figure 17 shows, this increase in air piston amplitude means that U'_o must be negative for a period of somewhat less than half of each cycle. The strong effect of the standing waves in the air chamber at resonance is to literally suck the air piston toward the chamber for each half cycle and push it outward for the other half at a velocity much higher than could be predicted from the mass flow rate of air through the siren. With no damping the wave equation predicts infinite velocity for any value of the forcing function (the integrated effect of the variable pressure at the upstream face of the rotating disc) (2). It is evident that there is some damping; otherwise the output intensity level would be infinite, which it is not. If the value of the forcing function were known for one situation, the damping could be determined for that case and it would be reasonable to assume approximately the same damping for all other cases. Then U'_o at resonance could be estimated. However, the value of the forcing function at resonance is never

known, so the amount of damping, and consequently U'_o at resonance, remains indeterminate. Thus, at resonance, the predicted radiation patterns, calculated without considering resonance, show consistently lower intensities than the actual results

3. Radiation Patterns:

A general discussion of the mechanisms of acoustic wave attenuation will precede the remarks concerning the comparison of the predicted radiation patterns and those obtained from actual experiments. Certain important points covered in this discussion will be useful in explaining the differences between observed and predicted results

In some cases there is very little correlation between the measured and predicted results, thus opening two avenues for investigation:

1. Is there any reason to dispute the measured result?
2. Are the predicted results as good as possible or, in other words, do they allow for every factor?

With respect to the predicted results, let us first analyze Equation C.10 in Appendix C, which is the basis for calculating intensity:

$$I = \frac{\rho_o c k^2 U_o^2 a_2^4}{8r^2} \left[\left(\frac{a_1}{a_2} \right)^2 \frac{2J_1(ka_1 \sin\theta)}{ka_1 \sin\theta} - \frac{2J_1 ka_2 \sin\theta}{ka_2 \sin\theta} \right]^2 \quad (4)$$

The right hand bracketed factor, which accounts for directivity, is indisputable because it is assumed we are dealing with a single frequency. The only term open to question is U_o, the velocity

amplitude of the air particles at the siren exit and this has been previously discussed. Equation 4 predicts intensity at a particular distance, r, from the source. It only allows for spherical divergence and does not account for any losses over the path travelled by the sound wave to that distance.

No losses were considered initially because of the relatively small distances with which this experiment is concerned. The change in intensity of the attenuated wave due to losses from viscous absorption and heat conduction, expressed in decibels, is given by (12):

$$\Delta IL = 10 \log e^{-2\alpha x} = -8.7\alpha x \qquad (5)$$

where:

x = distance from the source in meters

α = attenuation coefficient

The attenuation coefficient, α, is given by:

$$\alpha = \frac{\omega^2}{2\rho_o c^3}\left[\frac{4\eta}{3} + \frac{k(\gamma-1)}{c_p}\right] \qquad (6)$$

where:

η = shear coefficient of viscosity

k = thermal conductivity of fluid

γ = ratio of specific heats

c_p = specific heat at constant pressure

From Table 9.1 of Reference (12), for air at 20° C and P_o = 1 atmosphere, the classical calculation of α/f^2 is 1.37×10^{-11} and the observed value is 2×10^{-11}. Using the higher value, and computing ΔIL

at the highest experimental frequency, where the loss will be the greatest,

$$\Delta IL = -8.7\alpha x = -(8.7)(2\times10^{-11})(1.517\times10^{4})^{2}(0.16) = 6.4\times10^{-3}\text{db} \quad (7)$$

Because this loss is much smaller than the experimental error, it will still be neglected.

Extrapolation of curve (A) in Figure 9.5 of Reference (12) for total attenuation due to molecular thermal relaxation, viscous absorption, and heat conduction at 15,000 cps gives intensity loss equal to 0.4 db/meter or 6.4×10^{-2} db at a distance of 16 cm. Again, this loss is smaller than the experimental error and will be neglected.

The only remaining potential source of error in predicted intensity must come from the effects of non-linearity or "finite amplitude," and a general discussion of nonlinear sound propagation will be included here (13), (14).

A high amplitude sound wave will deform toward a stable sawtoothed shape. "Finite amplitude" distortion, which is the change in wave form from any generated shapeto the stable sawtoothed shape, may be attributed to two causes:

1. Sound consists of longitudinal vibrations and therefore the alternating air particle velocity is parallel to the direction of wave propagation. Because the pressure is in phase with the velocity, the pressure maxima and minima travel respectively with the velocity of sound plus and minus the particle velocity.

2. Temperature increases with increasing pressure and because

the velocity of sound is proportional to the square root of absolute temperature, the local wave velocity is greater than average at pressure maxima and less at pressure minima.

These two factors are additive. Thus pressure maxima overtake pressure minima, creating a steep pressure front at the leading edge of an acoustic wave. The strength of this front is a function of the attenuation characteristics of the medium and the amplitude of the wave. In the process of forming the sawtoothed wave, energy must be transferred from the fundamental component into the higher harmonics. In accordance with Equations 5, 6, and 7, there will be a much greater intensity loss due to the higher frequencies than was originally predicted. There will also be a sharp pressure discontinuity across the shock front, with associated losses. It is obvious at this point, even qualitatively speaking, that the best position for testing the gas turbine blade is as near the source as possible to take advantage of the sharp pressure discontinuity and to minimize the losses from high frequency, finite amplitude attenuation. It is not so apparent, but equally true, that the right hand bracketed factor of Equation 4 is no longer indisputable, but, as a matter of fact, it might contain serious errors. The sawtooth wave form may be considered to be made up of an infinite series of sine waves of frequencies corresponding to the harmonics of the fundamental, and this will lead to a much more complicated directivity pattern than the one used in Equation 4, where only the fundamental frequency was considered. It is even possible that the difference between the measured directivity pattern and the directivity pattern predicted on the basis of the fundamental

frequency alone might be a measure of the finite amplitude effect.

The distance from the source at which the stable sawtooth wave is attained is a function of both the form of the wave generated by the source and its amplitude. Because of microphone limitations it was impossible to observe the waveform at the source. The open-area-of-ports curve for the chopper is nearly sinusoidal. Therefore, it was assumed that a sinusoidal wave was generated at the source (1). This waveform and the extremely high amplitude of the source indicate that it is a good assumption to consider that the waves deform to the stable sawtooth shape as they leave the stationary disc. They remain sawtoothed as they propagate. See Figures 8(b) and (c) through 12(b) and (c).

The mechanism of the attenuation of high frequency, high intensity waves of finite amplitude will now be discussed.

A high amplitude plane wave of stable, sawtooth, shape will attenuate in amplitude according to the relation (14):

$$\frac{dp}{p} = - \frac{(\gamma+1)\, p\, dx}{\gamma \lambda P_o} \qquad (8)$$

where: P_o is atmospheric pressure

p is acoustic pressure amplitude

x is the distance

γ is the ratio of specific heats

λ is the sound wavelength

For non-plane waves the change in wave amplitude also results from the divergence of the wave. This divergence effect can be

be modeled by considering that the high amplitude wave is propagated in a horn in which the area, S, of an equiphase surface of the wave varies with distance, x, away from the sound source. A general expression for the area as a function of distance is:

$$Sg^2(x) = S_o \tag{9}$$

where: $S = S_o$ at $x = x_o$ and thus $g(x_o) = 1$.

The total change in amplitude with distance from the source is the combination of that caused by high amplitude attenuation from Equation 8 and that caused by divergence from Equation 9.

$$\frac{dp}{p} = \frac{dg}{g} - \frac{(\gamma+1)p\,dx}{\gamma\lambda P_o} \tag{10}$$

Equation 10 can be integrated to give (14):

$$p = \frac{p_o g(x)}{1 + \frac{\gamma+1}{\gamma\lambda P_o} p_o \int_{x_o}^{x} g(x)dx} \tag{11}$$

where p is the acoustic pressure amplitude in a sound wave at distance x from the source and p_o is the acoustic pressure amplitude at $x = x_o$.

In the limit, as p_o becomes very large, p takes a value at distance x which cannot be exceeded, no matter how large p_o becomes. This value of acoustic pressure p at distance x can be called the limiting pressure, p_l, given by:

$$p_l = \frac{\gamma\lambda P_o g(x)}{(\gamma+1)\int_{x_o}^{x} g(x)dx} \tag{12}$$

Equation 12 is perfectly general as it stands. It could be used for either plane wave or spherical wave propagation depending on the form of g(x). A plane piston source moving in a rigid baffle approximates a plane source near its surface and a spherical source at large distances. For a plane piston the dividing distance between the near field and the far field for acoustic purposes is (14):

$$R_n = \frac{\pi D^2}{4\lambda} \tag{13}$$

where D is the diameter of the piston source.

In this thesis the siren was modeled as a "ring source," which is a modification of plane piston source theory as explained in Appendix C. For a ring source, then, the dividing distance, R_{nr}, between the near field and far field is:

$$R_{nr} = \frac{\pi(D_1^2 - D_2^2)}{4\lambda} \tag{14}$$

where D_1 is the outer diameter and D_2 is the inner diameter of the ring.

To apply the finite amplitude limits to the siren ring source it is a good approximation to apply the plane wave limit version of Equation 12 to the near field and the spherical wave limit to the far field by matching the two limits at the distance R_{nr} (14).

For a plane wave g(x) = 1. Thus Equation 12 takes the form:

$$P_1 = \frac{\gamma \lambda P_o}{(\gamma+1)(x-x_o)} \tag{15}$$

in the near field. Equation 15 indicates that the limiting pressure

may be unlimited at the source where $x = x_o$, but at any other distance it decreases inversely as the distance measured in wavelengths. In air at a normal atmospheric pressure of 10^6 microbars Equation 15 can be expressed as:

$$P_1 = \frac{1.4 \times 10^6}{2.4} \left[\frac{\lambda}{x - x_o} \right] \tag{16}$$

or:

$$P_1 = 0.58 \times 10^6 \frac{1}{n} \tag{17}$$

where n is the number of wavelengths from the source.

For a spherical wave, r should be substituted for x and $\frac{1}{r}$ for g(x) in Equation 12 before integrating it. The resulting expression for the far field limiting pressure is:

$$P_1 = \frac{\gamma P_o}{\gamma+1} \frac{1}{\frac{r}{\lambda} \log_e \frac{r}{r_o}} \tag{18}$$

where r is the distance from the center of divergence and r_o is the distance from the center to the surface of the sound source (14).

Equation 17, plotted as curve (a), and Equation 18, plotted as curve (b), are expressed in decibels of sound pressure level versus the log of the distance from the source expressed in wavelengths at 15,095 cps in Figure 18. The two limiting curves are matched at R_{nr}, given by Equation 14. Predicted curves of sound pressure level versus distance in wavelengths from the source are plotted for each 10 decibels of source strength from 210 db down to 150 db. The 16 cm and 32 cm distances, expressed in wavelengths, of the microphone from the source

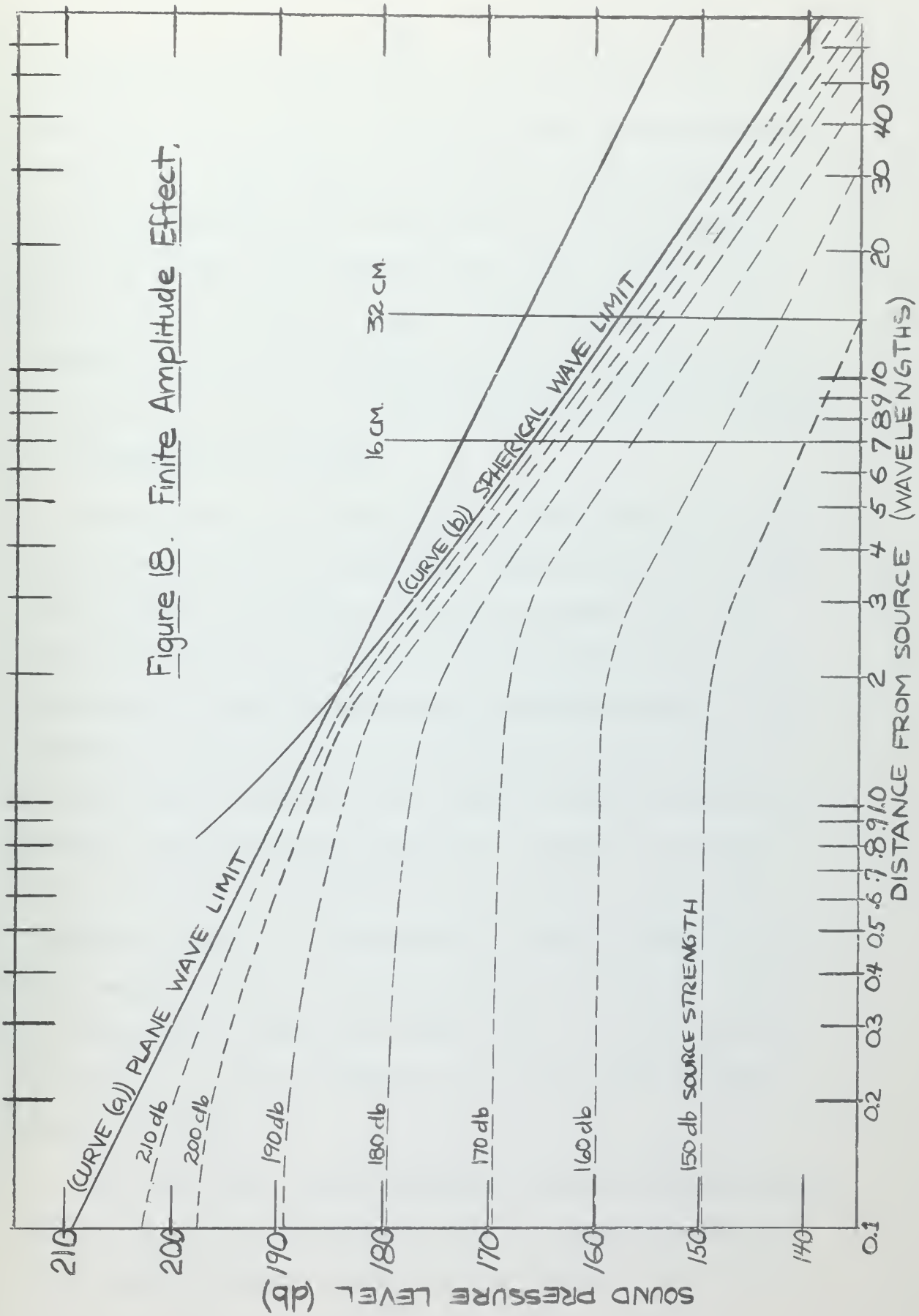

Figure 18. Finite Amplitude Effect.

are indicated on the figures since these distances were used in the experiments in this thesis. It can be seen that the predicted sound pressure level versus distance curves approach the limiting curves (a) and (b) asymptotically. Most important, it can be seen that the curves through a 60 db range of source level converge at the 16 cm and 32 cm locations to ranges of only 25 db and 22 db respectively. Thus, there comes a point at which substantially no increase in level at the 16 cm and 32 cm distances could be obtained by increasing the source power.

These remarks on the finite amplitude effect have been included because the results of the experiments conducted on the air chopper indicate that it has affected the results obtained. It has been shown that the higher the source strength the greater the rate of attenuation will result at distances of several wavelengths; often substantially greater than 6 db per distance doubling. Since the microphone used to measure the air chopper's output was necessarily located at some distance from the source, frequently the readings taken at 16 cm and 32 cm differed by more than 6 db. This great difference can often be attributed either solely or partially to the finite amplitude effect. In the discussion of the plotted results at each frequency, Figures 8(a) through 12(a), to follow, specific reference will be made to examples of the finite amplitude effect whenever appropriate.

The second avenue to be investigated, because of the discrepancy between the measured and predicted results, concerned the validity of the measured results. Was the observed intensity level a true

measure of the radiation pattern?

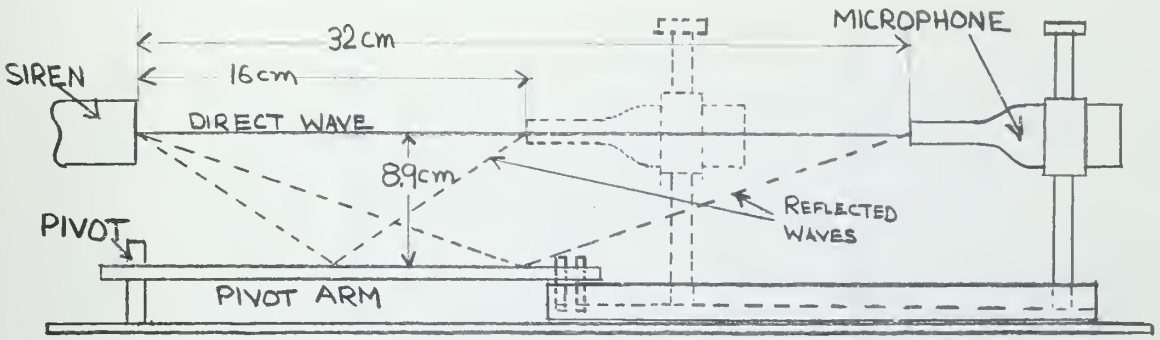

Figure 19 Schematic of Microphone Mount

The microphone was mounted so that it could be rotated in the horizontal plane containing the siren axis, and positioned at any radius from 0 to 32 cm as illustrated in Figure 19. With this mounting arrangement it was possible for the sound waves to reflect off the pivot arm. Thus the measured intensity level is the sum of the intensity levels of the direct and reflected rays. To predict the effect of the reflected ray it is necessary to estimate its phase and strength relative to the direct ray.

Since the frequency of the sound wave and the difference in distance traveled by the direct and reflected sound waves are known, the phase difference between the two rays can be computed. These phase differences are recorded in Table II. The phase relationship between the direct and reflected waves at 16 cm and 32 cm for each frequency influences the experimental radiation patterns. This is discussed in the following section, which compares actual and predicted results.

TABLE II

		16 cm			32 cm		
F(cps)	λ(cm)	Δd(cm)	$\Delta\lambda$(cm)	$\Delta\Phi$ ($^\circ$)	Δd	$\Delta\lambda$	$\Delta\Phi$
Frequency	Wave-length	Distance Difference	Wavelength Difference	Phase Differ			
7220	4.75	7.9	1.66	238	4.6	0.98	353
8440	4.07	7.9	1.93	335	4.6	1.12	43
12347	2.78	7.9	3.12	43	4.6	1.65	234
15095	2.27	7.9	3.48	173	4.6	2.01	3
15170	2.26	7.9	3.50	180	4.6	2.02	7

The relative strength of the reflected ray is a function of the difference in number of wavelengths traveled, the reflection coefficient of the pivot arm (assumed to be 1), and the angle, Θ_r, from the siren axis to the radius joining the center of the siren and the point where reflection occurs.

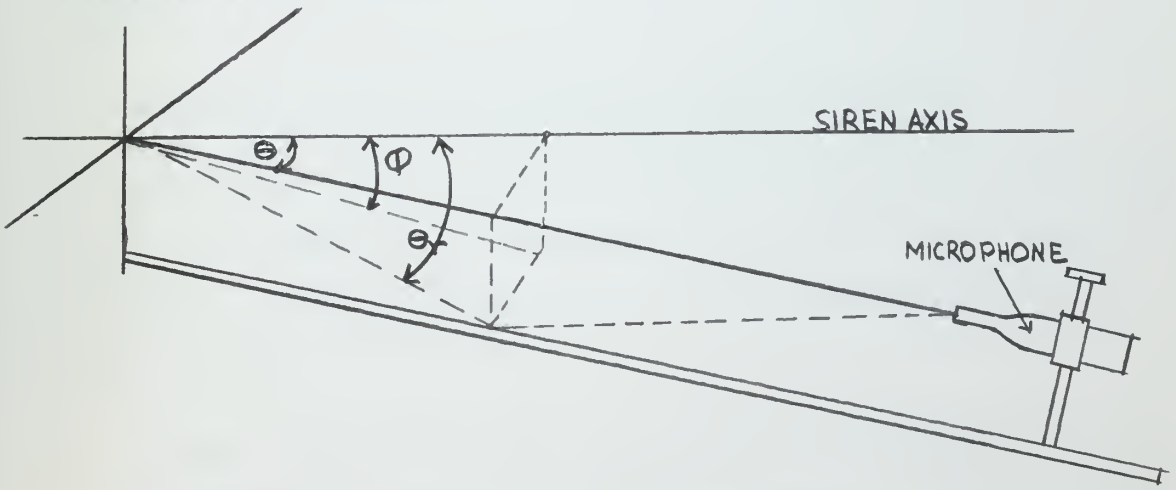

Figure 20 Θ_r, Directivity for Reflected Wave

From Figure 20, $\Theta_r = \cos^{-1}\left[\cos\Phi \cos\Theta\right]$. Values of Θ_r for various values of Θ are recorded in Table III.

TABLE III

Θ	0°	10°	20°	30°	40°	50°	60°	70°	80°	90°
Θ_r (at 16 cm)	48°	48.6°	50°	54.5°	59.1°	64.5°	70.5°	76.8°	83.3°	90°
Θ_r (at 32 cm)	29°	30.5°	34.5°	40.7°	48°	55.7°	64.0°	72.6°	81.25°	90°

Because of the axial symmetry of the directivity pattern, the intensity level of the reflected ray may be estimated by reading the intensity level from the radiation pattern plot for the desired frequency at the angle, Θ_r, and correcting this value for the difference in distance traveled by the direct and reflected rays. This method was used qualitatively to estimate the relative strength of the two rays. The effect of reflection for each frequency is discussed in the following section.

4. Comparison of Actual and Predicted Radiation Patterns:

Now that some of the important general effects which could cause differences between the experimental and predicted results have been discussed, their actual application to the results of this thesis will be shown.

Figures 8(a) through 12(a) contain plots of predicted radiation patterns (smooth solid lines) and actually measured radiation patterns (points connected with zig-zagging dashed lines). The experimental

points were connected with the dashed lines for clarity, to indicate those measured at 16 cm radius and those at 32 cm. Since readings were taken only at each 10°, it is by no means certain that the actual radiation pattern follows the dashed lines. There is even the possibility of nulls occurring between points shown connected by a straight line. Thus, the dashed lines should not be taken too literally as accurately representing the experimentally determined radiation pattern.

In all of the radiation pattern plots, Figures 8(a) through 12(a), a particular phenomenon is observed. In the vicinity of the axis (0°) the actual results are quite close to, or less than, the predicted results. However, at greater angles off the axis the actual results are generally much larger than the predicted results, particularly at resonant frequencies.

This phenomenon is caused by the "finite amplitude" effect mentioned above. In the vicinity of the axis the source is strongest (possibly about 200+ db). We have seen that the finite amplitude attenuation effect is stronger with more powerful sources, so we can conclude that near the axis the strong central lobe is attenuated more than any other lobe of a given radiation pattern. Conversely, the weaker side lobes are not so strongly attenuated by the finite amplitude effect. The overall result is to smooth out or equalize the lobes of each experimentally observed radiation pattern. This would not have occurred had the sound pressure level measurements been made with a microphone very near the chopper. However, since measurements were taken at several wavelengths from the source, this equalizing of lobes was inevitable because of the effect of finite amplitude

attentuation.

Figures 8(a) through 12(a) will now be individually discussed to explain additional ways in which each was particularly significant.

Figure 8(a), 8,440 cps, nozzle installed:

1. Figure 7 indicates that 8,440 cps is a resonant condition. The experimentally determined intensities are all higher than the predicted intensities. This result is not surprising in view of the previous remarks on resonance effects.

2. The lobing trends of the predicted directivity patterns are not shown by the experimental results. The predicted directivity patterns were based on the fundamental frequency alone. Since the stable sawtooth waveform has high harmonic content, the directivity portion of Equation 4 is influenced by a number of frequencies. The overall effect of these harmonics is, then, to fill in the null areas between the lobes predicted by the fundamental frequency and thus to "smooth" the actual directivity pattern.

Figure 9(a), 12,347 cps, nozzle installed:

1. Figure 7 indicates that 12,347 cps is a resonant condition. It is not surprising, then, that the experimental intensity readings are higher than those predicted.

2. The observed directivity pattern agrees better with the predicted pattern than at 8,440 cps. The power and intensity readings indicate that this is not as strong a resonance at all angles as that at 8,440 cps. Since the source strength is less here, the finite

amplitude attenuation is less and the waves contain fewer significant harmonics. Thus, the directivity portion of Equation 4 agrees better with that based on the fundamental frequency.

3. The plots of the actual results at the 16 cm and 32 cm radii indicate that there was generally a greater than 6 db loss per distance doubling at this frequency. As shown in Table II, the reflected wave is in phase with the direct wave at 16 cm and out of phase with the direct wave at 32 cm. This reflection effect, coupled with greater attenuation at the longer radius from the finite amplitude effect, were responsible for the greater than 6 db difference between the 16 cm and 32 cm radiation patterns.

Figure 10(a), 15,095 cps, nozzle installed:

1. Figure 7 indicates that 15,095 cps is not a resonant frequency for the siren.

2. The plots of the actual results at the 16 cm and 32 cm radii indicate that there was greater than 6 db loss per distance doubling near the axis, and nearly no loss per distance doubling at angles of 50° - 90°. Near the axis, since the major lobe of the radiation pattern is much stronger than the others, the finite amplitude effect of causing greater than 6 db loss per distance doubling predominated. At the greater angles off the axis where the 16 cm and 32 cm readings were about the same, the finite amplitude effect was not shown since the side lobes are naturally of lower intensity. Table II, however, indicates that at this frequency the waves reflected off the microphone mount were about exactly out of phase with the direct waves at 16 cm, while

at 32 cm the reflected and direct waves were nearly perfectly in phase. Thus, at these larger angles off the axis the reflection effect predominates. The 16 cm intensity was reduced and the 32 cm intensity was augmented until they became about the same.

Figure 11(a), 7,220 cps, no nozzle:

1. Figure 7 indicates that 7,220 cps is a resonant frequency. The experimentally determined intensities are all higher than the predicted intensities. At this particular frequency there is the largest overall difference between observed and predicted results. Since 7,220 cps is one of the strongest resonances, considering the average of the sound pressure levels at all angles, this unpredictably large difference between observed and predicted intensities is, again, not surprising.

2. The lobing trends of the predicted directivity patterns are not shown by the experimental results. The reasons for the discrepancy at this frequency are the same as those given in remark 2 of the discussion of Figure 8(a), above. The fact that there is even greater disagreement at 7,220 cps than at 8,440 cps could have been expected since the former frequency had the stronger overall resonance effect and, thus, more significant harmonics.

3. At angles of greater than 50° off the axis there was much less intensity loss per distance doubling. Table II indicates that at this frequency, 7,220 cps, the waves reflected off the microphone mount are out of phase with the direct waves at 16 cm, while the two are exactly in phase at 32 cm. At these larger angles off the axis,

then, the reflection effect causes the 16 cm intensity to be reduced and the 32 cm intensity to be augmented so that they are both nearly the same at each angle. This same effect occurred in measurements taken at 15,095 cps.

Figure 12(a), 15,170 cps, no nozzle:

1. Figure 7 indicates that 15,170 cps is not a resonant frequency for the siren. Except for the fact that intensities at this configuration are generally higher than those read at 15,095 cps with the nozzle in place, the same general discrepancies exist at 15,170 cps, and for the same reasons. The discussion of Figure 10(a), above, applies exactly to the results shown in Figure 12(a), then, with the slight difference that the influence of reflection off the microphone mount began at 40° off the axis for the latter figure.

5. Efficiency:

The results tabulated in Table I show that quite low efficiencies were obtained at all frequencies, particularly at those near 15,000 cps which were not at resonance. This, as mentioned in the Introduction, was an expected result since this siren is one of inherently low efficiency. The high intensities at all frequencies depended on the supply of as much as 29,500 watts of "air power," an extraordinarily high amount for a siren of such small dimensions. At this supply of air power the siren put out 6419 watts of acoustic power for an efficiency of 21.7%. This was the highest efficiency measured for the siren in its original form, and it occurred at 7,220 cps, a resonant condition. While this efficiency does not seem high, it was measured while the

siren was putting out an estimated 190 + decibels of sound pressure level at 1 cm distance, a very high intensity. For the purposes of this siren, high intensity was the only desirable result. It can be concluded that to get high intensity from a small siren, efficiency must be low, simply because a high amount of air power must be supplied to the siren. Since the siren is physically small, the mass flow rate of air through it is relatively low and a high amount of air power can be achieved only through use of a high air supply pressure (100 psi in this case). Thus, to make a small siren emit a very high amount of acoustic power, it must be supplied with high pressure air and operate at low efficiency.

Much lower efficiency exists when the siren is operating in a non-resonant condition. At these conditions, approximately the same air power is provided to the siren as at resonance, but the acoustic power out is much less. In one case an efficiency of as little as 2.1% was computed, corresponding to an acoustic output power of 573 watts. This occurred when the siren was operated at 15,095 cps with the nozzle in place. It is an obvious conclusion that the siren is much more efficient at resonance since nothing more is supplied to the siren, but a good deal more power out is achieved.

Table I also shows that output power and efficiency are higher when the nozzle is not used, both at non-resonance and at resonance. One primary reason for this is that the exit area of the nozzle, 0.6 square inch, is smaller than the total port area, 0.7325 square inch. Thus, the nozzle had the smallest area in the siren, choking the air flow even more than it would have been choked by the siren ports

if the nozzle had not been used. The result is shown in Figures 8(a) through 12(a) where it can be seen that the mass flow rate through the siren is lower whenever the nozzle is used. As stated in the Introduction, a basic premise of good siren design is to have the highest possible mass flow rate. This was born out by experiments with this and other sirens (1), (4).

Even if the exit area of the nozzle had been larger than the siren port area the nozzle would very likely still have detracted from the siren's output. This is so because the nozzle is such a bad approximation to a properly designed horn. A well designed horn, which would both concentrate the chopper's output on a blade undergoing test and provide a smooth transition of the acoustic pulses from the port area to the infinite area of the atmosphere, is shown in Appendix E, Figure E.1.

A particularly surprising result is shown by comparing the power and efficiency columns in Table I for the 16 cm radius with those at 32 cm. It would be expected initially that power and efficiency should be the same at both radii, assuming spherical spreading. It has been shown in the remarks on finite amplitude attenuation, however, that attenuation occurs at greater than 6 db per distance doubling for very strong sources. For this reason, power and efficiency should have been less at 32 cm; certainly not more as generally shown in Table I.

There are two possible explanations for this observed phenomenon. First, the integration to obtain power out, by the method shown in

Appendix D, was based on sound pressure level readings taken at 10° intervals on the 16 cm and 32 cm radii. In retrospect, it seems that these readings were too coarse. If measurements had been taken at intervals of 5° or less, the integrated overall power values at 16 cm and 32 cm would have been more accurate, and thus more likely to bear the correct relationship to each other. In other words, the power values given in Table I at both 16 cm and 32 cm can, at best, only be called estimates.

The second reason for the surprising result that power calculated at 32 cm was greater than that at 16 cm, disregarding the above reason of too little intensity data, results from the phenomenon of reflection off the microphone mount. The previous discussion of Figures 8(a) through 12(a) points out that reflection affected the radiation patterns at angles off the axis of greater than about 40° to 50°. At these higher angles, generally less than 6 db loss existed between the 16 cm and 32 cm radii at a given angle. Since this small loss per distance doubling generally existed through at least half of each radiation pattern, it is obvious that integration over a hemisphere would give greater power at the outer radius than at the inner. To further substantiate the contention that reflection caused the generally higher power values at the 32 cm radius, note that the only frequency at which the 32 cm power was lower than the 16 cm power was 12,347 cps. Table II shows that the reflected waves were in phase with the direct waves at 16 cm and out of phase at 32 cm. This is precisely the relationship which would cause lower power at the larger radius.

Modified Air Chopper:

For a closed right circular cylinder of constant radius, the siren chamber dimensions used with Equation 3 predict that a reduction of length of one-half inch will cause a resonant frequency shift as shown in Figure 16(a).

In the model, specific modes of resonance can be defined and a resonant mode frequency shift can be predicted. However, the closed right circular cylinder model does not perfectly represent the chamber. Therefore, specific modes cannot be defined and modal frequency shift cannot be predicted for the siren chamber. It can be stated that for a given resonant mode, decreasing the length of the chamber will increase the resonant frequency.

A comparison of Figures 15(a) and 15(b), or Figures 16(a) and 16(b), illustrates that changing the length of the siren chamber with the plug shown in Figure 14(a) does change resonant frequencies. Since the resonant modes cannot be identified in the actual siren chamber it is impossible to indicate the resonant frequency shift for a given mode.

The results of using the slug shown in Figure 14(b) are illustrated by Figure 15(c). Both slugs changed the chamber length by the same amount. A comparison of Figures 15(b) and 15(c) indicates that the resonance patterns for the two slugs are similar. Therefore it can be said that the length of the chamber is the dominant dimension affecting resonant frequencies.

The general tendency of decrease in sound pressure level with

increasing frequency, shown in Figures 15(a), (b), and (c), can be attributed to:

1. The major lobe of the directivity pattern becomes narrower at higher frequency. The microphone was located at 15^{o} off the axis for these measurements to keep it out of the air stream. As shown in the predicted radiation patterns of Figures 8(a) through 12(a), at 15^{o}, sound pressure level will decrease with increasing frequency.

2. Mass flow rate decreases slightly with increasing frequency.

3. Finite amplitude attenuation is greater at higher frequencies.

The resonances are undoubtedly more pronounced than shown in Figures 15(a), (b) and (c). Figure 18 shows that the difference between two intensity levels decreases with increasing distance from the source. The microphone was located at a distance of 20 cm from the source. Therefore, at the siren exit the sound pressure level at a resonant frequency is much greater than at an adjacent non-resonant frequency. Gas turbine blades tested at the siren exit would obtain the full benefit of the resonant effect.

CONCLUSIONS

1. Sirens have resonant frequencies at which the output intensity is significantly higher than adjacent non-resonant frequencies, for the same operating conditions.

2. The frequencies at which resonance occurs are determined primarily by the length of the air chamber immediately upstream of the rotating disc.

3. To force a physically small siren to emit high intensity sound requires a high pressure air supply and results in low efficiency operation.

4. The effects of finite amplitude attenuation preclude estimating the intensity level near the source on the basis of intensity level measured several wavelengths from the source.

5. The source strength of the siren cannot be determined theoretically at a resonant frequency because it is impossible to predict U_o', the amplitude of the air particle velocity at a resonance.

6. Intensity varies directly with mass flow rate. To obtain maximum mass flow rate, the cross-sectional flow area at every point in the siren should be greater than the maximum total open port area.

7. The finite amplitude effect causes distortion of directivity patterns measured at distances of several wavelengths from high intensity, high frequency sound sources.

8. The best results for fatigue testing can be obtained with the blade located as near as possible to the high intensity acoustic source

to minimize intensity loss from finite amplitude attenuation and spherical divergence.

RECOMMENDATIONS

Proposed Modifications to the General Electric Siren:

1. The controllable length chamber shown in Figure 13 should be incorporated into the siren. This will permit the operator to tune the chamber so that its resonance will correspond to the siren operating frequency necessary to test a gas turbine blade at one of its natural frequencies. Thus, an intensity level will be available at all frequencies which is appreciably higher than that with the present siren.

2. The frequency range of the siren may be extended to 22,500 cps by using new discs with 30 ports in them.

3. To concentrate the acoustic power output on the blade and to provide a smooth transition of the sound waves from the siren exit to the atmosphere, the horn designed in Appendix E should replace the stationary disc of the present siren.

General Recommendations Pertaining to Apparatus and Experimental Procedure:

1. The microphone should be capable of measuring the intensity level at the source with a flat response over the entire frequency range of interest.

2. The microphone should be mounted so that reflection will not interfere with the measurements.

3. Because of finite amplitude attenuation, the acoustic power output of a high intensity siren cannot be predicted on the basis of intensity levels measured several wavelengths from the source.

Therefore a better estimation of the acoustic power output might be obtained from a thermodynamic analysis of the flow through the siren (5).

APPENDIX

APPENDIX A

METHOD FOR CALCULATING MASS FLOW RATE

The air mass flow rate was measured with an ASME square-edged orifice meter with flange taps (10). The meter was constructed of 2-inch pipe, and all dimensions are as specified in Reference 10. The orifice used had a diameter of 1.29 inches. Mass flow rate was calculated using the following equations:

$$w_t = 0.4219\, D_2^2 K Y \sqrt{\frac{p_1}{T_1} G y \Delta p} \qquad (A.1)$$

where:

w_t = mass flow rate of air, lb_m/sec
D_1 = pipe diameter, inches (2.067 inches)
D_2 = orifice diameter, inches (1.29 inches)
K = flow coefficient, dimensionless, based on β and Reynolds Number (Table 6 of Ref. 10)
Y = expansion factor, dimensionless, based on $\frac{\Delta p}{p}$ and β (Fig. 37 of Ref. 10)
p_1 = static pressure before orifice, inches Hg absolute
T_1 = temperature before orifice, ^{o}F absolute
G = specific gravity of gas (air = 1.00)
y = supercompressibility factor, dimensionless, based on pressure and temperature (Fig. 11, Ref. 10) (1.00)
Δp = pressure drop across orifice, inches Hg = $P_1 - P_1'$

$$\beta = \frac{D_2}{D_1} = \frac{1.29}{2.067} = 0.625$$

For 2-inch pipe and $\beta = 0.625$, the maximum value of K is 0.7090, for a Reynolds Number of 10,000 and the minimum value of 0.6608, for a Reynolds Number of 10,000,000. Reynolds Number is unknown in these

experiments but, although the tabulated range (in Ref. 10) is from 10,000 to 10,000,000, the variation in K is small. By selecting a mean value of K, which is 0.6849, calculations were made which had a 3.52% maximum uncertainty in the determination of K. This degree of precision was satisfactory for our calculations. If more accuracy had been required an iterative solution could have been done, using Reynolds Numbers obtained from the first approximate values of w_t based on a mean value of K, to obtain successively better values of K.

Incorporating the constant parameters into Equation (A.1), the final, simplified, relationship used for calculating mass flow rate was:

$$w_t = 0.480 Y \sqrt{\frac{P_1}{T_1} \Delta P} \qquad (A.2)$$

APPENDIX B

METHOD OF CALCULATING "AIR POWER" AND "EFFICIENCY"

To determine the efficiency of the air chopper it was necessary to know the power in as well as the acoustic power out. The power supplied to the chopper consists of two parts. The major portion comes from the power represented by the air supplied at high pressure, or "air power." A minor contribution comes from the electric motor which drives the rotating disc.

A. Air Power

"Air power," or ideal power available from the high pressure air supply, is obtained by multiplying the mass flow rate of the air by the work done in expanding it from its high pressure state to the atmosphere isentropically. In other words, it is the same power that would be obtained by expanding the air from a given high pressure state to the atmosphere through an ideal, isentropic nozzle.

$$P_{air} = Aw_t(h_{o2} - h_{3s}) \qquad (B.1)$$

where:

P_{air} = air power, watts
A = constant = 1054 watts/BTU/sec
w_t = total air mass flow rate, lb_m/sec
h_{o2} = enthalpy of the air as it enters the chopper air chamber, based on the stagnation pressure and temperature there (see Fig. 6), BTU/lb_m.
h_{3s} = enthalpy of the air at atmospheric pressure and at the same entropy value as h_{o2}, BTU/lb_m.

B. Efficiency:

The air power calculated as in Equation (B.1), represents the largest amount of power which theoretically could be extracted from the available air supplied to the air chopper. In the air chopper, however, the total mass flow rate of air, w_t, is composed of a part which does no work at all, the leakage air. In addition, port resistance and flow losses detract from perfect energy conversion. Finally, since there is choked flow in the chopper ports, there are shock losses in the portion of the air flow which is converted to accoustic power.

The power supplied to run the rotating disc in the chopper is hard to estimate. Even if the electric power into the drive motor were measured it would be hard to say how much of it is lost in the 25:1 gearbox. Since the drive motor is rated at 3 hp, in no case could more than 2238 watts be provided by that source. This is less than 10% of the air power and, in any case, only the chopper itself is of interest, rather than the motor and gearbox. For purposes of this thesis, then, motor power will be ignored and efficiency will be expressed as:

$$\eta = \frac{\text{accoustic power out}}{\text{air power}} \qquad \text{(B.2)}$$

rather than:

$$\eta = \frac{\text{accoustic power out}}{\text{air power + motor power}} \qquad \text{(B.3)}$$

APPENDIX C

RADIATION FROM A RING SOURCE

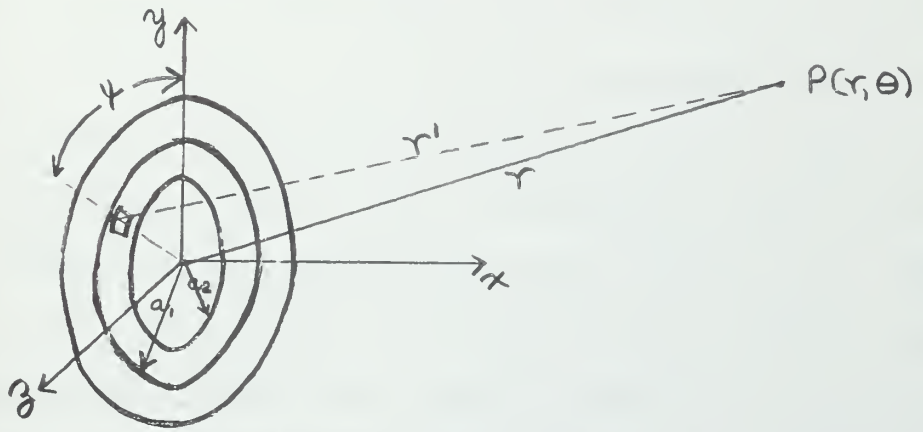

Figure C.1 Coordinate system used in deriving the radiation characteristics of a Ring Source.

The pressure produced at any point by an extended surface source is the sum of the pressures that would be produced by an equivalent assembly of simple sources. For example, each infinitesimal element of area $d\bar{s}$ of a vibratory surface mounted in a infinite baffle contributes an element of pressure $d\bar{p}$ given by (12):

$$d\bar{p} = \frac{i\rho_o ck}{2\pi r'} (\mathcal{U}\, d\bar{s})\, e^{i(wt-kr')} \qquad (C.1)$$

where r' is the distance from the surface element to the point in the medium where $d\bar{p}$ is measured.

Consider a rigid annular ring mounted flush with the surface of an infinite baffle, and vibrating with simple harmonic motion $u = U_o \cos wt$. Assume the outer and inner radii to be a_1 and a_2 respectively, and that its vibrating surface lies in the yz plane, with its center coinciding with the origin of coordinates. The radiation will then be symmetric about the x axis, so that it is sufficient to

specify the position of a point in space by the spherical coordinates r and Θ , where r is the radial distance from the center of the annular ring, and Θ is the angle between the radius vector and the x axis, as in Figure C.1. Let positions on the surface of the annular ring be specified by the polar coordinates σ and ψ , where σ is the radial distance from the center of the annular ring and ψ is the angle between the corresponding radius vector and the y axis. The area ds of a surface element of the annular ring is $\sigma d\sigma d\psi$. Letting r' represent the distance from a surface element ds to a point $P(r,\Theta)$ in the medium, the acoustic pressure $d\bar{p}$ produced at this point by the motion of ds is

$$d\bar{p} = \frac{i\rho_o ck}{2\pi r'} U_o ds\, e^{i(wt-kr')} \qquad (C.2)$$

Since the motion of every surface element of the annular ring is normal to its surface, the scalar product in Equation C.1 has been replaced by $U_o ds$. The total pressure $\bar{p}$ at the point $P(r,\Theta)$ is the integral of this expression over the surface of the annular ring.

The distance r' is equal to

$$r' = (r^2 + \sigma^2 - 2r\sigma \sin\Theta \cos\psi)^{\frac{1}{2}} \qquad (C.3)$$

If r is large compared with a_1 and a_2, r' is approximately equal to

$$r' \approx r - \sigma \sin\Theta \cos\psi + \ldots. \qquad (C.4)$$

At considerable distances from the annular ring, the amplitude of the pressure produced by any single surface element differs only very slightly from that produced by any other element, so the distance r'

in the denominator of Equation (C.2) can be satisfactorily approximated by using only the first term of the series (C.4) i.e., $r' = r$. On the other hand, the relative phase of the pressures produced at $P(r, \theta)$ by any two surface elements depends on the difference in distance of the two elements, and for distant points this distance is practically independent of r. As a consequence at least two terms of the series must be used for the phase factor of Equation (C.2), i.e., for the r' appearing in the exponential. The approximate expression for the pressure at considerable distances from the annular ring is therefore

$$\bar{p} = \frac{i\rho_o ck}{2\pi r} U_o e^{i(\omega t - kr)} \int_{a_2}^{a_1} \sigma \, d\sigma \int_0^{2\pi} e^{ik\sigma \sin\theta \cos\psi} \, d\psi \qquad (C.5)$$

The expression $\int_0^{2\pi} e^{ik\sigma \sin\theta \cos\psi} \, d\psi$ can be integrated using the general relation

$$J_m(x) = \frac{(-i)^m}{2\pi} \int_0^{2\pi} e^{ix\cos\psi} \cos(m\psi) \, d\psi \qquad (C.6)$$

then

$$\int_0^{2\pi} e^{ik\sigma \sin\theta \cos\psi} \, d\psi = 2\pi J_o(k\sigma \sin\theta) \qquad (C.7)$$

The second integration of Equation C.5 can be carried out by using the relation $\int x J_o(x) dx = x J_1(x)$. Then

$$2\pi \int_{a_2}^{a_1} \sigma J_o(k\sigma \sin\theta) d\sigma = 2\pi \left[\frac{a_1^2 J_1(ka_1 \sin\theta)}{ka_1 \sin\theta} - \frac{a_2^2 J_1(ka_2 \sin\theta)}{ka_2 \sin\theta} \right] \qquad (C.8)$$

Substitution into Equation C.5 gives for the complex pressure

$$\bar{p} = \frac{i\rho_o ckU_o}{2r} e^{i(wt-kr)} \left[a_1^2 \frac{2J_1(ka_1 \sin\theta)}{ka_1 \sin\theta} - a_2^2 \frac{2J_1(ka_2 \sin\theta)}{ka_2 \sin\theta} \right] \tag{C.9}$$

The pressure amplitude P is

$$P = \frac{\rho_o ckU_o}{2r} \left[a_1^2 \frac{2J_1(ka_1 \sin\theta)}{ka_1 \sin\theta} - a_2^2 \frac{2J_1(ka_2 \sin\theta)}{ka_2 \sin\theta} \right] \tag{C.9a}$$

and the intensity I is

$$I = \frac{P^2}{2\rho_o c} = \frac{\rho_o ck^2 U_o^2 a_2^4}{8r^2} \left[\left(\frac{a_1}{a_2}\right)^2 \frac{2J_1(ka_1 \sin\theta)}{ka_1 \sin\theta} - \frac{2J_1(ka_2 \sin\theta)}{ka_2 \sin\theta} \right]^2 \tag{C.10}$$

To predict intensity according to Equation C.10 at a given frequency, distance, and angle, it is necessary to calculate U_o, the amplitude of the annular ring velocity. The annular ring is composed of the 20 equally spaced ports in the outer, or fixed, disc. These ports can be thought of as 20 small "air pistons" of constant area, A. The volume flow, q, through each "piston" is:

$$q = AU_o e^{iwt} \tag{C.11}$$

The velocity, $U_o e^{iwt}$, in Equation C.11 is assumed to have only positive values, since the total volume flow rate of air through the siren, Q, is in one direction only and never reverses itself. It can be assumed, however, that $U_o e^{iwt}$ has an instantaneous zero value as each port is closed and a maximum value as the port is fully opened by the motion of the inner, rotating siren disc. The resulting effect is a sinusoidal velocity of amplitude U_o, varying about an average

velocity of air flow, $\tilde{U}_o$,

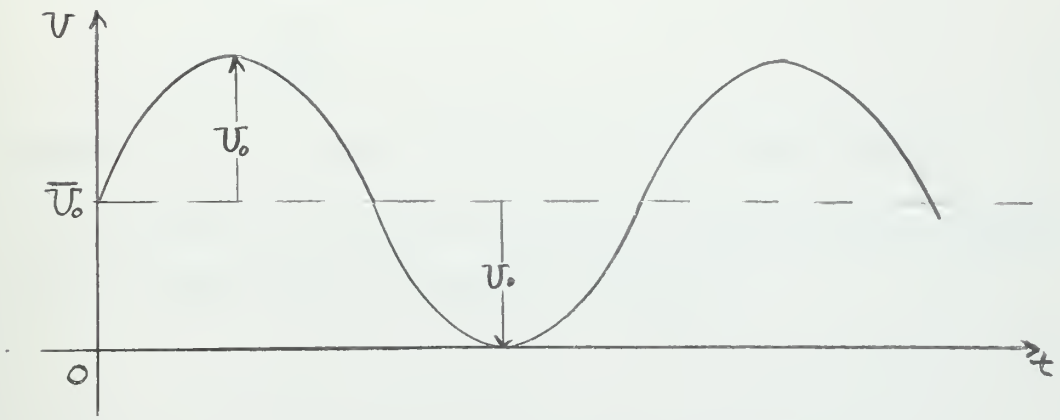

Figure C.2 Air Particle Velocity in Air Pistons

as shown in Figure C.2. The velocity amplitude of the annular ring is the same as the velocity amplitude, U_o, of the twenty individual ports, or "air pistons," comprising it. For the annular ring, then,

$$Q = 20q = 20\, AU_o e^{iwt} \tag{C.12}$$

The mass flow rate of air through the siren ports, W_p, was measured for each experiment. The volume flow rate of air, Q, can thus be obtained from the known W_p:

$$Q = \frac{W_p}{\rho}, \text{ where } \rho = \frac{P_2}{RT_2} \tag{C.13}$$

Since Q, from Equation C.13, is an average value, Equation C.12 could also be written:

$$Q = 20\, A\overline{U_o e^{iwt}} \tag{C.14}$$

where $\overline{U_o e^{iwt}}$ is the average velocity of the air through the ports.

From Figure C.2 it can be seen that $U_o e^{iwt} = \tilde{U}_o = U_o$, and Equation C.14 can be written:

$$Q = 20AU_o \tag{C.15}$$

Combining Equations C.13 and C.15:

$$U_o = \frac{W_p}{20A\rho} \qquad (C.16)$$

where the total port area, 20A, equals 0.7325 square inches

The value of U_o given by Equation C.16 may be used in Equation C.10 to obtain values of predicted intensity.

APPENDIX D

ACOUSTIC POWER OUTPUT OF PULSED-AIR VIBRATION EXCITER

Sound Pressure Level (Ref $P_o = 0.0002$ dynes/cm^2) was measured every 10^o on a circular arc of 16 cm radius from 0^o, on the siren axis, around to 90^o, perpendicular to the siren axis. The Sound Pressure Level was converted to intensity according to the relation

$$SPL = IL = 10 \log \frac{I}{I_o} \qquad (D.1)$$

where SPL = Sound Pressure Level

IL = Intensity Level

I = Intensity (watts/cm^2)

I_o = Reference Intensity 10^{-16} watts/cm^2

Axial symmetry of the acoustic pressure field was assumed and no reflection was considered. The surface area of a hemisphere of 16 cm radius was divided into elements; the first element was 5^o wide, the next 8 elements were each 10^o wide, and the tenth element 5^o. Thus each elemental area was centered about an angle at which the intensity was known. The area of each elemental area was calculated.

$$A_e = 2\pi R^2 \Delta\theta \sin\theta \qquad (D.2)$$

where A_e = elemental area (cm^2)

R = radius = 16 cm

$\Delta\theta$ = width of elemental area

θ = angle from the axis to the center of the elemental area

The acoustic power transmitted across each elemental area was obtained by multiplying the intensity there by the elemental area. Summing the ten elemental powers so obtained gave the total acoustic power output of the siren. The same procedure was repeated for a radius of 32 cm.

APPENDIX E

HORN DESIGN FOR A PULSED-AIR VIBRATION EXCITER

For an exponential horn, (see Eq. 9.17, Ref. 2,)

$$S = S_T e^{mx} \tag{E.1}$$

where S = cross sectional area at x

S_T = cross sectional area of throat

m = flare constant

x = distance from throat

The cutoff frequency of the horn must be lower than any operating frequency (2). Since it was desired to operate this horn over a range of siren operating frequencies above 7500 cps, this was selected as the cutoff frequency. The flare constant equals, (see Eq. 9.28, Ref. 2,)

$$m = \frac{4\pi F_c}{c} = \frac{4\pi(7500)}{344.8} = 272\ m^{-1} = 6.92 in^{-1} \tag{E.2}$$

The total throat area was assumed to equal the maximum open port area, $S_t = 0.732\ in^2$. Because it was desirable to concentrate the intensity of the acoustic field of the siren, it was decided to restrict the horn mouth area to a circular cross section 1.5 inches in diameter, the approximate length of the blades to be tested. Mouth area is equal to

$$S_m = \frac{\pi D^2}{4} = \frac{\pi(1.5)^2}{4} = 1.762\ in^2 \tag{E.3}$$

The length of the horn from Eq. E.1 is equal to

$$l = \frac{1}{m} \ln \frac{S_m}{S_t} = \frac{1}{6.92} \ln \frac{1.762}{0.732} = 0.127 \text{ in.}$$

Because this length is so short, it was decided to incorporate the horn in the stationary disc of the siren. (See Fig. E.1)

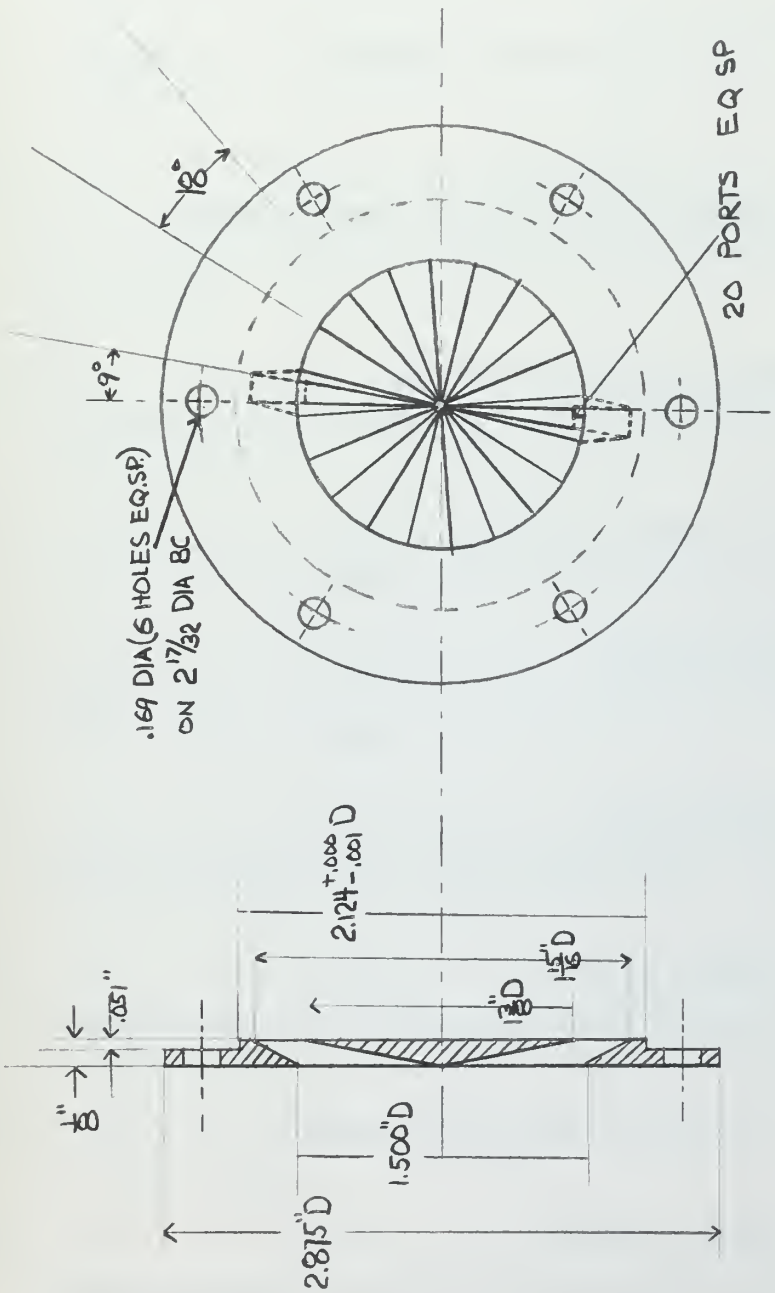

FIGURE E.1 MODIFIED STATIONARY DISC WITH HORN INCORPORATD IN EACH OF 20 PORTS

BIBLIOGRAPHY

1. Lunday, G. P., Investigation of Air Flow Mechanism and Sonic Output of an Axial Flow Sound Generator, S. M. Thesis, MIT, M. E., 1950.

2. Beranek, L. L., Acoustics, McGraw-Hill, New York 1954, p. 268-71, p. 286-287.

3. Cole, J. N., Powell, G. P., Oestreicher, H. L., and von Gierke, H. E., Acoustic Siren for Generating Wide-Band Noise, Journal of the Acoustical Society of America, Vol. 35, No. 2, Feb. 1963, p. 179-188.

4. Forney, D. M., Jr., Acoustical Fatigue Test Procedures Used in Aircraft Industry and Their Limitations, WADC TR 59-676, March 1961, p. 344.

5. Jones, R. Clark, A Fifty Horsepower Siren, Journal of the Acoustical Society of America, Vol. 18, Oct. 1946, p. 371-378.

6. Allen, C. H., and Rudnick, I., A Powerful High Frequency Siren, Journal of the Acoustical Society of America, Vol. 19, Sept. 1947, p. 857-865.

7. Allen, C. H., and Watters, B. G., Siren Design for Producing Controlled Wave Forms at High Intensities, Journal of the Acoustical Society of America, Vol. 31, No. 2, Feb. 1959, p. 177.

8. Allen, C. H. and Watters, B. G., Siren Design for Producing Controlled Wave Form with Amplitude Modulation, Journal of the Acoustical Society of America, Vol. 31, No. 4, April 1959, p. 463-469.

9. Morse, P. N., Vibration and Sound, McGraw-Hill, New York, 1948, p. 245, p. 399-401.

10. Leary, W. A. and Tsai, D. H., Metering of Gases by Means of the ASME Square-Edged Orifice with Flange Taps, Sloan Laboratory for Automotive and Aircraft Engines, MIT, July 1, 1951.

11. Klint, R. V., Truman, J. C., and Martin, J. R., A Pulsed-Air Vibration Technique for Testing High-Performance Turbomachinery Blading, General Electric Company Report No. 60-RL-24556, June 1960.

12. Kinsler, L. E. and Frey, A. R., Fundamentals of Acoustics, Second Edition, John Wiley & Sons, New York, 1962, p. 166-168, p. 225-226, p. 232.

13. Rudnick, I. On the Attenuation of High Amplitude Waves of Stable Saw-Tooth Form Propagated in Horns, Journal of the Acoustical Society of America, Vol. 30, No. 4, April 1958, p. 339-342.

14. Allen, C. H., and Weiner, S. D., Study Directed toward Optimization of Operating Parameters of the EMAC Probe for the Remote Measurement of Atmospheric Parameters, Bolt, Beranek and Newman, Inc., Report No. 1056 of Sept. 1963, Cambridge, Mass, p. 61-79.